Retention and diffusion of radioactive and toxic species on cementitious systems: Main outcome of the CEBAMA project

Bernd Grambow, M Lopez-García, J Olmeda, M Grivé E A, Nicolas C.M. Marty, S. Grangeon, F Claret, S Lange, G Deissmann, M. Klinkenberg, et al.

Manuscript for Applied Geochemistry

Retention and diffusion of radioactive and toxic species on cementitious systems: main outcome of the CEBAMA project

B. Grambow* (10), M. López-García (1), J. Olmeda (1), M. Grivé (1), N.C.M. Marty (2), S. Grangeon (2), F. Claret (2), S. Lange (3), G. Deissmann (3), M., Klinkenberg (3), D. Bosbach (3), C. Bucur (4), I. Florea (4), R. Dobrin (4), M. Isaacs (5), D. Read (5), J. Kittnerová (6), B. Drtinová (6), D. Vopálka (6), N. Cevirim-Papaioannou (7), N. Ait-Mouheb (7), X. Gaona (7), M. Altmaier(7), L. (8,9), B. Lothenbach (8), J. Tits (9), C. Landesman (10), S. Rasamimanana (10), S. Ribet (10)

(1) Amphos21, Spain,

(2) BRGM, 3 avenue Claude Guillemin, 45060 Orléans cedex 2,France,

(3) FZ Jülich, Germany,

(4) RATEN, Romania,

(5) University of Surrey, & National Physical Laboratory, United Kingdom,

(6) CTU, Prague, Czech Republic,

(7) Karlsruhe Institute of Technology, INE, Germany,

(8) EMPA, Switzerland,

(9) Paul Scherrer Institute, Switzerland,

(10) Subatech (IMT Atlantique, University of Nantes, IN2P3, CNRS) Nantes, France.

*corresponding author, grambow@subatech.in2p3.fr, 4 rue Alfred Kastler – La Chantrerie, 44307 Nantes, France

Highlights

- understanding anion retention in cementitious materials
- reducing uncertainties with respect to radionuclide behaviour in hardened cement pastes
- justifying assumptions used when representing radionuclide migration in safety assessments
- improving databases for assessing adsorption of radionuclides in fresh and degraded cement systems

Abstract

Cement-based materials are key components in repository barrier systems. To improve the available knowledge base, the CEBAMA (Cement-based materials) project aimed to provide insight on general processes and phenomena than can be easily transferred to different applications. A bottom up approach was used to study radionuclide retention by cementitious materials in the European CEBAMA project, encompassing both individual cement mineral phases and hardened cement pastes. Solubility experiments were conducted with Be, Mo and Se under high pH conditions to provide realistic solubility limits and radionuclide speciation schemes as a prerequisite for meaningful adsorption studies. A number of retention mechanisms were addressed including adsorption, solid solution formation and precipitation of radionuclides within new solid phases formed during cement hydration and evolution. Sorption/desorption experiments were carried out on several anionic radionuclides and/or toxic elements which have received less attention than metals to date, namely: Be, Mo , Tc, I, Se, Cl, Ra and ^{14}C. Solid solution formation between radionuclides in a range of oxidation states (Se, I and Mo) and the main components (OH^-, SO_4^{-2}, Cl^-) of cementitious phases (AFm, $Ca_4Al_2(OH)_{12}\cdot SO_4\cdot 6H_2O$) were also investigated.

Keywords

Cement-based materials, radionuclide and toxic element retention, sorption, solubility, hydrolysis, diffusion, CEBAMA

Introduction

Cement-based materials are widely used as waste forms, backfill, seals, or as structural components in current and planned repositories for low, intermediate and high level radioactive waste (Glasser et al., 1989). Substantial data on these materials exists both in the nuclear and the civil engineering sectors but there are nevertheless, important gaps in our knowledge regarding their long-term performance. The European project CEBAMA was established to address key issues of relevance for long term safety and remaining scientific questions related to the use of cement-based materials as barrier in radioactive waste management. The research conducted was independent of specific disposal concepts and addressed the behaviour of cementitious materials in different host rocks considering where appropriate the likely presence of bentonite backfills. CEBAMA did not focus on one specific cement material, but rather aimed to provide insight into generic processes and phenomena that could then be transferred to different applications and repository projects.

Radionuclide retention in cementitious systems depends on the nature, charge and valence state of the radionuclide, on environmental conditions (cation and anion concentrations, Eh, pH, temperature), the type and degradation state of the cement pastes (see supplementary materials for definition) including carbonation, the presence of additives such as organic molecules (superplasticisers, retarders) and the water/cement ratio (Ochs et al., 2016). Cement pore water generates a high pH environment, which may reduce the solubility and hence migration of certain radionuclide species (Felipe-Sotelo et al., 2016, Felipe-Sotelo et al., 2017), but can increase mobility of anionic species. Anion retention has not been investigated to the same extend than that of cations.

The retention mechanism in any given situation depends on the total concentration of the investigated species, including radioactive and stable isotopes, and the solid to liquid ratio. For example, by using MoO_4^{2-} as a probe and supplementing adsorption isotherms with *in situ* time-resolved synchrotron-based X-ray diffraction, Ma et al. (2017) have identified three retention modes on AFm phases ($Ca_2(Al,Fe)(OH)_6]\cdot X\cdot xH_2O$ where X equals an exchangeable singly charged or half of a doubly charged anion) depending on total Mo concentration: edge adsorption at low Mo concentrations, interfacial dissolution-precipitation as an AFm-MoO_4 phase (AFm phase where some of the sulphate anions forming the AFm structure are substituted by molybdate anions) at higher Mo concentrations and solubility constrained by precipitation of $CaMoO_4$ for the highest Mo concentrations investigated. In contrast, Marty et al. (2018), using a flow-through experimental system with an initial Mo

concentration around 5 mM, did not observe dissolution/ precipitation, but only interlayer adsorption. This was attributed to the fact that, in batch experiments, a fast AFm equilibration led to increase Ca and Al concentration that induced dissolution/precipitation phenomena. The present work covers several retention processes such as by adsorption, co-precipitation and precipitation of radionuclide-bearing solids.

A bottom-up approach was used extending from radionuclide retention studies on synthesized individual hydrated cement phases to hardened cement pastes (HCP) covering a range of compositions (CEM I, CEM II, CEM V and a low pH cement formulation). Upon closure of a nuclear waste repository, influx of groundwater will alter the cement-based materials and could potentially compromise radionuclide containment. Therefore, the impact on retention of radionuclides of various geochemical alteration processes, such as carbonation and alteration of cement-based materials were also investigated. Since unsaturated conditions with relative humidity (RH) values as low as 50% may arise during repository development, some experiments were performed in humid air at corresponding RH values.

The individual hydrated cement phases were studied comprising the major phases of a CEM I cement, excluding portlandite ($Ca(OH)_2$), as no significant interaction of the latter and the radionuclides of interest is expected (Ochs et al., 2016). Calcium silicate hydrate (C-S-H) and calcium aluminate as AFm or AFt, with general formula $Ca_6(Al,Fe)_2X_3(OH)_{12}\cdot xH_2O$, X being one divalent or two monovalent anions (Champenois et al., 2012, Goetz-Neunhoeffer and Neubauer, 2006); these phases together constitute ≈60% of bulk hydrated cement pastes and provide favourable sites for the adsorption of radionuclides (Evans, 2008 and Ochs et al., 2016). The properties of these phases are strongly dependent on their crystallographic structure, including crystal size and the nature of the layer charge (e.g., isomorphic substitutions, lattice vacancies). A good understanding of their interaction with radionuclides is vital for building a safety case for a geological disposal facility. As many data for radionuclide retention on cementitious materials have already been determined (e.g. Bradbury and Sarrot, 1995, Wieland, 2014, Ochs et al., 2016), only those radionuclides regarded as being of high priority from the safety perspective and which have not yet received sufficient attention in the past, especially Be(stable), ^{14}C, ^{129}I, ^{36}Cl, ^{79}Se, ^{93}Mo, ^{226}Ra and ^{99}Tc have been studied in this work. They are largely but not exclusively anionic species and are perceived as potentially more mobile under repository conditions. Depending on the redox state of the geochemical and engineered barrier environment, the key anionic species are Cl^-, I^-, IO_3^-, Se^{-2}, SeO_3^{-2}, SeO_4^{-2}, MoO_4^{-2}, $^{14}CO_3^{-2}$ and TcO_4^-.

Important interactions of anions are expected to occur onto AFm phases, hydrotalcite-like phases ($4CaO\cdot Al_2O_3\cdot 13–19\ H_2O$) and AFt phases. AFt phases have the general formula $Ca_6(Al,Fe)_2X_3(OH)_{12}\cdot nH_2O$, X being one divalent or two monovalent anions. They are characterized by a pillar structure consisting of positively charged $[Ca_3(Al,Fe)(OH)_6\cdot 12H_2O]^{+3}$ columns. The positive charge on the columns is compensated by exchangeable negatively charged $[3/2X\cdot nH_2O]^{-3}$ anions in channels. The most important AFt phase is ettringite ($X=SO_4$) which forms quite rapidly in the early stages of cement hydration (Taylor, 1997). AFm phases also formed during cement hydration, they have a lamellar structure composed of a positively charged main layer and a negatively charged interlayer, $[X\cdot nH_2O]^{-2}$, X : 2 singly charged or 1 doubly charged anion (Buttler et al., 1959). The general structural formula of an AFm is $[Ca^{+2}_4(Al^{+3}_xFe^{+3}_{(1-x)})_2(OH)_{12}]\cdot X\cdot nH_2O$, where the main layer species are put between brackets and $X\cdot nH_2O$ represents the hydrated exchangeable “interlayer anions” (n is the number of water molecules).These exchangeable interlayer anions compensate for the positive layer charge induced by the presence of trivalent cations in the layers, providing AFm with an anion-exchange capacity. Natural anionic species competing for exchange sites include OH^-, CO_3^{2-}, SO_3^{2-}, SO_4^{2-}, $S_2O_5^{-2}$ etc. There are two types of exchange sites identified for fixation of anions: surfaces ion exchange and interlayer anion exchange sites (Ma et al., 2017, Ma et al., 2018).

C-S-H phases precipitate during the hydration of Portland cement and blended cements. C-S-H are characterized by calcium to silica molar ratio (Ca/Si) between 0.7 and 1.7. They are nanocrystalline and disordered phases whose structure is thought to be close to tobermorite $Ca_5Si_6O_{16}(\underline{OH})_2\cdot nH_2O$ (although some authors also propose jennite $Ca_9Si_6O_{18}(OH)_6\cdot 8H_2O$). The variability in the Ca/Si ratio is due to variable degree of polymerization of the Si chains, and subsequent charge compensation by interlayer Ca. At the highest Ca/Si ratios,

nanocrystalline $Ca(OH)_2$ can be present. Surface charge of a solid phase may influence in a great extent the interactions that occur between the solid surface and the species in solution. At low Ca/Si ratios, negative surface charge is observed on C-S-H, while at higher Ca/Si ratios the sorption of Ca^{+2} results in an apparent positive surface charge of C-S-H (Churakov et al., 2014). Hence, the variation on composition causes significant changes in their properties as adsorbent. Due to the importance of C-S-H phases in cementitious materials, Ra^{2+}, I^-, MoO_4^{-2}., SeO_3^{-2} and SeO_4^{-2} retention was studied for different Ca/Si ratios (corresponding to different stages of alteration of cements).

Mineral precipitation is a potentially significant retention process for both cationic and anionic radionuclide species (Ma et al., 2019). In order to avoid misinterpretation of solubility derived data as 'sorption' processes, adsorption studies were performed at sufficiently low concentrations to avoid precipitation. Specific solubility studies in cementitious systems were conducted for $CaMoO_4$ (powellite), BeO(cr) and α-$Be(OH)_2$ (cr). The implications of calcite solubility on data interpretation for $^{14}CO_3^{-2}$ sorption is also addressed.

Pure hydrated cementitious phases and HCP were synthesized and characterized. Advanced micro-analytical and spectroscopic techniques were used in order to derive detailed process understanding (see supplementary information).

Experimental

The experimental techniques used include the fabrication of pure phases and solid solutions, solubility tests, adsorption and diffusion studies. Different cement formulations are used. A large quantity of analytical techniques have been used to characterise aqueous and solid phases before and after the experiments. Details are given in the supplementary information.

Results and Discussion

Solubility studies

The low solubility of certain radionuclide phases in high pH solutions can provide an effective retention mechanism. For example, precipitation of calcite at the high Ca concentrations present in cement pore water can significantly reduce the mobility of $^{14}CO_3^{-2}$. In this work, the solubility of several potentially important radionuclide-bearing solid phases has been determined.

$CaMoO_4$

Under cementitious conditions (pH>9, [Ca]=1-20 mM), powellite ($CaMoO_4$(s)) is believed to be the solubility-controlling phase under all stages of cement degradation (Kindness et al., 1994). In this case, molybdenum solubility is very sensitive to differences in calcium concentrations. The conditions under which powellite might precipitate cover a wide range of pH and Eh, suggesting the stability of this phase in cements-based materials. Only at the more advanced stages of cement degradation and strongly reducing conditions would Mo solubility be controlled by MoO_2(s) (Grive and Olmeda, 2016). Berner (2014) conducted solubility and speciation calculations in cementitious pore waters using the Nagra/PSI Chemical Thermodynamic Data Base for Mo. He established the total dissolved concentration of MoO_4^{2-} equal to $7.2 \cdot 10^{-6}$ M with $CaMoO_4$(s) as the stable solid; MoO_2(s) was stable only below -750 mV/SHE.

Powellite solubility was evaluated using prepared AFt equilibrated waters. These solubility tests confirmed that experimental data can be accurately described using the solubility constant reported in the bibliography (log_Ks,25°C = 7.90±0.33 from Thermochimie Database vs 9.b.0; (Giffaut et al., 2014).

α-Be(OH)$_2$(cr) and BeO(cr)

Solubility data obtained in this work (see details in supplementary data, 4) confirm the amphoteric character of Be(II), with a solubility minimum at pH_m 9 (with pH_m=- log [H^+]). At this pH_m, [Be(II)] in equilibrium with BeO(cr) and α-Be(OH)$_2$(cr) is ≈$10^{-7.5}$ and ≈10^{-7} M, respectively. The hydrolysis constant previously reported for Be(OH)$_2$(aq) in potentiometric studies is substantially overestimate (Bruno, 1987, Chinea et al., 1997, Kakihana and Sillen, 1956). The combination of solubility data determined in this work, slope analyses, solid phase characterization and ^{9}Be NMR allow comprehensive chemical, thermodynamic and (SIT) activity models for the system Be^{+2}–Na^+–K^+– H^+–Cl^-–OH^-–H_2O(l) (see Cevirim-Papaioannou et al., 2019, this special issue). Additional experiments conducted in the presence of carbonate (see Figure 1) highlight that, within the boundary conditions expected in cementitious systems, carbonate cannot outcompete hydrolysis and that the aqueous speciation of Be(II) is dominated by the anionic species $Be(OH)_3^-$ and $Be(OH)_4^{-2}$.

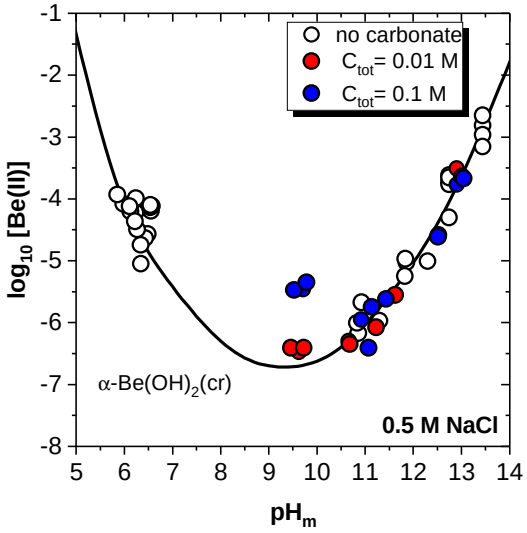

Figure 1. *Solubility of α-Be(OH)$_2$(cr) in 0.5 M NaCl–NaOH-NaHCO$_3$–Na$_2$CO$_3$ solutions at 9.5 ≤ pH_m ≤ 13 and C_{tot} = [HCO_3^-] + [CO_3^{2-}] = 0, 0.01 and 0.1 M. Solid line corresponding to the solubility calculated with the thermodynamic model derived in* (Cevirim-Papaioannou et al., 2019) *(this special issue)*

Characterization and solubility product of pure AFm phases

Pure AFm phases containing selenate, selenite, selenide and molybdate have been reported by to play a role in the retention of Se(IV) or Mo in cement systems (Felipe-Sotelo et al., 2016, Ma et al., 2017, Rojo et al., 2018). They appear to form at solution concentrations of Se or Mo lower than required for formation of pure $CaSeO_3$(s) or $CaMoO_4$(s), respectively. On the other hand side, pure Mo(VI)- and Se(VI)-AFm phases apparently are only able to form once surface sorption sites on the edges of the original S(VI)-AFm or Cl_2-AFm are saturated (Ma et al., 2017, Ma et al., 2018). In the present work pure S(VI)-AFm, S(IV)-AFm, S(II)-AFm, Se(IV), Se(VI) and the I-AFm were synthesised to allow comparison of the thermodynamic stabilities of Se- and I-containing AFm phases with the stabilites of AFm phases containing anions commonly present in cementitious environments under oxidizing and reducing conditions (L. Nedyalkova et al., 2019b). Most of the above-listed AFm phases were observed to crystallize in the rhombohedral $R\bar{3}$ space group with common position of the (110) reflection of the basal plane at ~31° 2Θ. Only the Se(IV)-AFm sample and the Se(VI)-AFm sample exhibit diffraction patterns corresponding to a symmetry lower than rhombohedral.

The S(VI)-AFm sample after drying was found to be a mixture of two phases, one with 12 H_2O molecules and an interlayer distance of 8.93 Å, and the other one with 14 H_2O molecules and an interlayer distance of 9.50 Å, the latter being more relevant in H_2O-saturated conditions. The rhombohedral crystal structure of S(VI)-AFm was refined by (Allmann, 1977). Diffraction data of the S(IV)-AFm sample revealed a hexagonal lattice with a rhombohedral space group. The interlayer distance was found to be 8.51 Å. Structure analysis suggests that the SO_3^{2-} anions are positioned parallel to the main layer at the center of the interlayer region (L. Nedyalkova et al.,

2019b). Diffraction patterns of the S(II)-AFm sample suggest a symmetry lower than rhombohedral. The use of a monoclinic unit cell however cannot satisfactorily explain the diffraction data. An ab-initio structure determination from the powder diffraction data using FOX (Free objects for Cristallography, Favre-Nicolin and Černý, 2002) revealed on average a rhombohedral lattice for this AFm phase with an interlayer distance of 10.33Å.

In the Se(IV)-sample the co-existence of two distinct Se(IV)-AFm hydrates was found (Latina Nedyalkova et al., 2019b) with rhombohedral and trigonal symmetries having interlayer distances of 11.05 Å and 9.65 Å, respectively, similar to the values of 11.03 Å and 9.93 Å reported by (Ma et al., 2018). The diffraction patterns found for Se(VI)-AFm phases suggest a symmetry lower than the previous AFm phases and correspond to an apparent monoclinic unit cell with an interlayer distance of 10.18 Å . The water content of the synthesized AFm phases was determined with thermogravimetry and dynamic vapor sorption (DVS). This information combined with the chemical composition of the solutions in equilibrium with the AFm phases allowed to determine solubility products (log K) using the thermodynamic modelling software GEMS (Kulik et al., 2013) and the NAGRA/PSI thermodynamic database (Hummel et al., 2002a, (Hummel et al., 2002b). Defining the solubility product of AFm phases, log_K_{so}, described by the equation (1):

$$Ca_4Al_2(OH)_{12}X\cdot nH_2O \Leftrightarrow 4Ca^{+2}+2Al(OH)_4^-+X^{-2}+4OH^-+nH_2O \quad , \qquad (1)$$

the following mean values were calculated: log_K_{s0}= -26.9 ± 0.9 (S(IV)-AFm), -27.8 ± 0.5 (I-AFm), -28.4 ± 1.4 (Se(IV)-AFm), 28.5 ± 1.4 (S(VI)-AFm), -29.2 ± 0.6 (Se(VI)-AFm) and -30.5 ± 0.8 (S(II)-AFm). These values are comparable with the solubility products for Se(VI)-AFm and Se(IV)-AFm obtained by Ma et al., (2018) reformulated to the above definition of log_K_{s0}.

Dissolution rates of AFm phases

Dissolution rates for AFm-Cl phases have been determined in flow-through tests at pH values ranging from 9.2 to 13 (Marty et al., 2017). For pH values from 10 to 13, congruent dissolution was observed (i.e. Ca/Al ratios close to 2 both for solids and outlet concentrations). In contrast, precipitation of amorphous Al-phases and possibly amorphous mixed Al/Ca phases was suspected at pH 9.2 leading to Ca/Al ratios higher than those of the initial solid determined from the outlet solutions. The far-from-equilibrium dissolution rate at pH values ranging from 9.2 to 13 and room temperature is given by log R = -9.23±0.18, with R values provided in $mol\cdot m^{-2}\cdot s^{-1}$, indicating complete dissolution in few days (I.e. high reactivity). Hence, AFm phases are only stable in cementitious systems under close to equilibrium conditions.

Exchange process of AFm phases with radionuclides of interest

Using the Cl^-/MoO_4^{-2} exchange on Afm-Cl as test case, flow-through experiments were conducted in alkaline conditions ((Marty et al., 2018; Grangeon and Marty, 2019). Experiments were performed using medium Mo concentrations (0.6–0.9 mM) under far-from-equilibrium conditions with respect to AFm (i.e. in conditions where precipitations of Cl-AFm and MoO_4-AFm are unexpected). A MoO_4^{-2}-rich solution was flowed through an AFm-Cl suspension and chemical parameters (pH and concentrations) were monitored at the output of a reactor. The MoO_4^{-2}/Cl^- and OH^-/Cl^- selectivity coefficients were determined by modelling MoO_4^{-2} and Cl^- concentrations as a function of time (GT model in Fig 2); there were found to be $10^{1.3}$ and $10^{-0.8}$, respectively. Nonetheless, it is also possible to model experimental data of Marty et al. (2018) using the solid solution approach described by Walker (2010) as show by the SS model in Fig 2. The SS model was an ideal solid solution with 3 end-members (Cl-AFm, OH-AFm and MoO_4-AFm). Whatever the modelling approach (GT or SS models), one mole of MoO_4^{-2} replaced two moles of Cl^-, as expected from the ratio of charges. However, exchange reaction implies that MoO_4^{-2} sorption is fast and reversible, i.e. that no structural incorporation or coprecipitation occurred. To verify this hypothesis, a molecular-scale understanding of the sorption is mandatory. To this end Marty et al., (2018) collected the X-ray scattering signal of the AFm-Cl before and after reaction with MoO_4^{-2}, and processed the data in the reciprocal (q) and real (r) spaces to first check for AFm-Cl purity (Fig. 3a) and then decipher the local order around sorbed Mo and the modifications of the unit cell induced by Mo sorption. In the r space, authors determined that MoO_4^{-2}

replaces Cl- in the interlayer and adopts a regular geometry, with the four Mo-O distances being equal to 1.78 Å (Fig 3b). In the q space, it could be shown that the incorporation of MoO_4^{-2} increases the layer-to-layer distance by 0.7-2.1 Å as compared to AFm-Cl (Fig. 3c). It is proposed that the heterogeneity in layer-to-layer distance results either from two different interlayer organizations of MoO_4^{-2} or from heterogeneous hydration state. At the crystal scale, it was observed that the Cl-/MoO_4^{-2} exchange involved interstratification of Mo- and Cl-rich interlayers. Authors found no evidence for sample recrystallization or secondary phase formation, possibly because the continuous solution renewing allowed keeping low Ca and Al concentration, thus preventing reaching supersaturation of any phase.

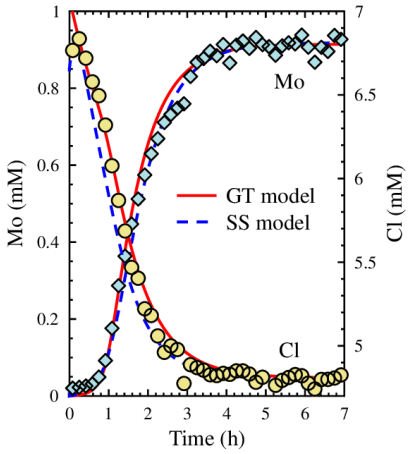

Fig. 2. Experimental (symbols) and modelled (lines) [Mo] (diamond) and [Cl] (circle) as a function of time of at the output of a reactor in which a solution containing Mo is flowed through an AFm-Cl suspension (modified from (Grangeon and Marty, 2019)).

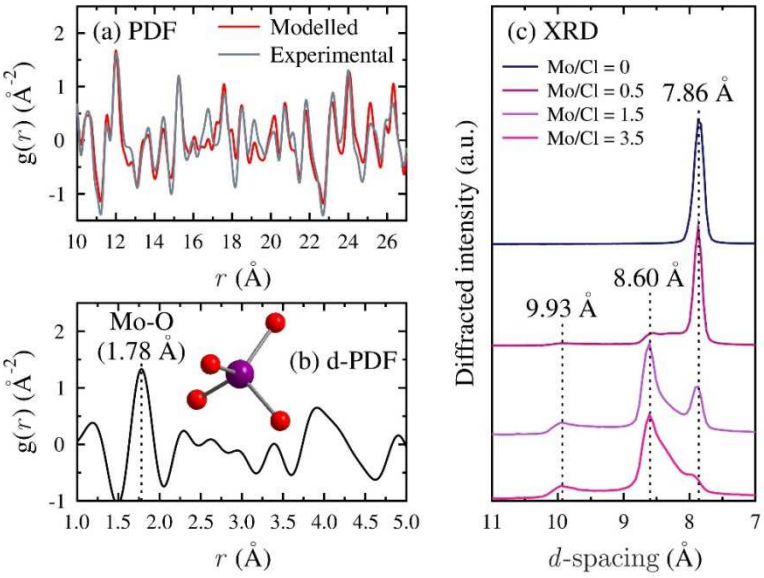

Fig. 3. (a): Experimental and modelled AFm-Cl PDF. (b): differential PDF (AFm-Cl minus a sample with Mo/Cl = 3.5). The Mo-O peak at 1.78 Å is diagnostic for MoO_4^{-2} (schematized in the inset). The peak at ~4 Å is due to Mo-Ca and Mo-Al correlations, consistent with MoO_4^{-2} in the interlayer mid-plane. (c): X-ray diffraction pattern of samples having Mo/Cl ranging 0-3.5. Peak asymmetry is due to interstratification (extracted from (Grangeon and Marty, 2019)).

Formations of solid solutions between AFm phases and radionuclides of interest

The results of the exchange experiments above provide for a more systematic approach describing solid solution formation. The formation of solid solution of the type SeO_3^{2-}–X^{n-} and I^--X^{n-} (with X^{n-} = SO_4^{-2}, SO_3^{-2}, $S_2O_3^{-2}$, CO_3^{-2}, OH^-) as the intercalating anions was examined. Samples with total selenite/iodide mole fractions ($x_{Se(IV)} = SeO_3^{-2}/(SeO_3^{-2}+X^{-n})$) of 0, 0.1, 0.3, 0.5, 0.7, 0.9 and 1 were synthesized. XRD analyses revealed solid solutions between the pairs: SeO_3^{-2}-SO_4^{-2}, I^--CO_3^{-2}, I^--OH^-_CO_3^{-2}, and I^--OH^-. A continuous solid solution was found between the end members Se(IV)-AFm and S(VI)-AFm, favoured by the similar rhombohedral symmetry, where the larger ionic radius of the SO_4^{-2} anion (2.58 Å) compared to the SeO_3^{-2} anion (2.39 Å) (Jenkins and Thakur, 1979) results in a continuous peak shift towards higher basal spacing (d-spacing values) with increasing amount of SO_4^{-2}. Continuous solid solution formation was also observed between the I^-–OH^-_CO_3^{-2} pair where the d value increases uninterrupted from 8.20 Å for the OH^-_CO_3^{-2}-AFm end member to 8.84 Å for the AFm end member.

Solid solution formation also takes place between the pairs I^--OH^- and I^--OH^-_CO_3^{-2}, favoured by the rhombohedral structure of all three end-members I^--AFm, OH^--AFm and hemicarbonate (OH^-_CO_3^{-2}-AFm). The increasing substitution of the larger I^- anion (2.10 Å) by the smaller OH^- anion (1.33 Å) is reflected by a gradual decrease of the interlayer distance from 8.84 Å in the I^--AFm phase down to 8.44 Å at a total iodide fraction of 0.1 (x_I = 0.1). At this composition a miscibility gap at very low I^- contents is observed. The solid solution formation between the I^--AFm and monocarbonate (CO_3^{-2}-AFm), is incomplete and a miscibility gap with the composition 0.5 ≤ $CO_3^{-2}/(2I^- + CO_3^{-2})$ exists (Fig. 3 b). An initial peak shift up to a composition of 0.3 ≤ $CO_3^{-2}/(2I^-+CO_3^{-2})$ is observed, suggesting that small amounts of the CO_3^{-2} anion (ionic radius 1.78 Å, Jenkins and Thakur, 1979) can be readily incorporated into the I^--AFm structure to form a mixed ($2I^-$-CO_3^{-2})-AFm phase. The solid solution is limited to compositions 0.5 ≤ $CO_3^{-2}/(2I^-+CO_3^{-2})$, where two coexisting phases - an ($2I^-$-CO_3^{-2})-AFm mixed phase and a CO_3^{-2}-AFm, indicate the presence of a miscibility gap. This miscibility gap could be related to the differences in the structure as monocarbonate has a triclinic structure, and to the planar arrangement of carbonate in the CO_3^{2-}-AFm interlayer which prevents the uptake of the larger I^- anion into the lattice. Comparable behaviour has been observed for chloride uptake by monocarbonate (Mesbah et al., 2011).

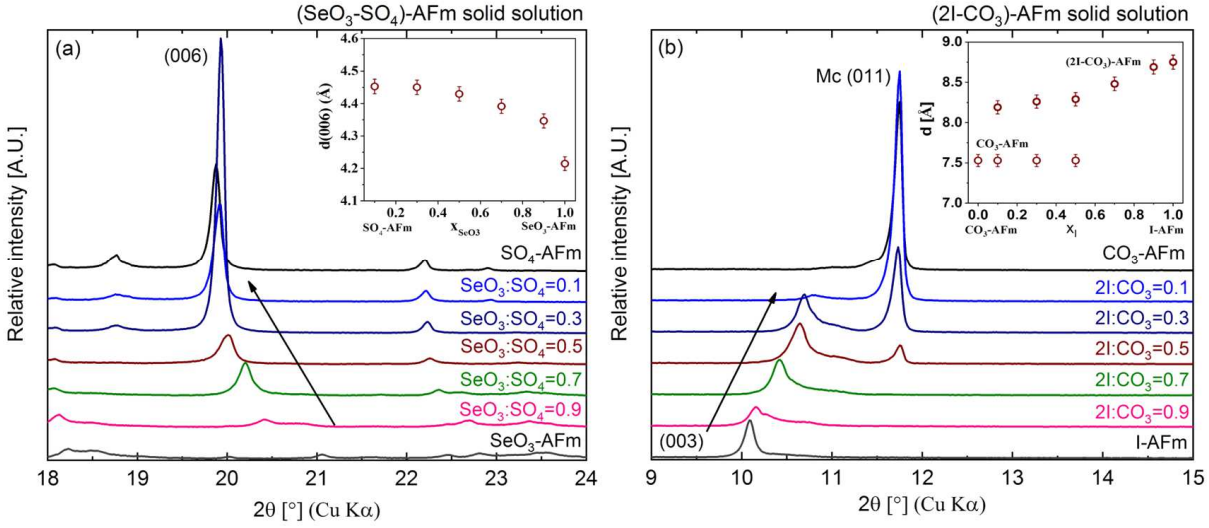

Figure 4 a and b: Evolution of the position of the basal reflection in the (SeO_3^{-2}-SO_4^{-2})-AFm (a) and the ($2I^-$-CO_3^{-2})-AFm (b) solid solution series. (b) modified from (L. Nedyalkova et al., 2019)

The solid solution behaviour observed in the XRD patterns was confirmed by FTIR analyses (L. Nedyalkova et al., 2019). In the (I^--OH^-_CO_3^{-2})-AFm solid solution series, the absorption band at 775 cm^{-1} caused by the Al-OH deformation vibration in the rhombohedral structure, gradually weakens and shifts towards 745 cm^{-1} corroborating the existence of a continuous solid solution.

Two coexisting phases can be distinguished clearly in the FTIR spectra of the I-CO_3 solid solution series. For compositions where x_I ≥ 0.7, the behaviour of the Al-OH absorption band is similar as observed in the (I^--OH^-_CO_3^-

^{2})-AFm solid solution series discussed previously, and only a single mixed phase is present. At the compositions below x_I = 0.5 additional absorption bands at ~948 cm^{-1}, ~875 cm^{-1} and ~667 cm^{-1} appear suggesting the presence of triclinic CO_3^{-2}-AFm in addition to the rhombohedral AFm phase.

Sorption distribution ratios (R_d) on individual cementitious phases and HCP for the compilation of sorption databases

Adsorption is a retention process qualitatively different from solid solution formation or precipitation as it only involves retention processes on the surface of existing solids. Both adsorption and solid solution formation can be treated mathematically in a similar way, if bulk phase atoms become accessible for exchange, as shown above for the 2 Cl^-/MoO_4^{-2} exchange in AFm-Cl^- planes. Consequently, as observed in the present work, both, a sorption and a solid solution model describe these exchange data equally well. Note however that these two phenomena should be distinguishable based on the aqueous concentration of AFm layer species (Al, Ca). Further work is required to test this hypothesis. The observations of (Ma et al., 2017, Ma et al., 2018) for fixation of MoO_4^{-2} or SeO_3^{-2} on AFm-Cl^- or AFm-SO_4^{-2} phases show that the adsorption process occurs at much lower radionuclide concentrations than the formation of pure AFm-SeO_3^{-2} or AFm-MoO_4^{-2} phases. If solid solution formation were to be the mechanism controlling molybdate ion uptake on AFm-Cl^- at low molybdate concentrations or selenite uptake on AFm-SO_4^{-2} at low selenite concentration in solution, one would expect a smooth transition in the corresponding solid solution controlled apparent sorption coefficients from the domain of solid solution formation at low radionuclide concentration to the domain of pure phase precipitation with increasing radionuclide concentrations. In contrast, the authors have observed a step increase of apparent R_d values, once AFm-MoO_4^{-2} is formed, indicating an adsorption/precipitation transition rather than a solid-solution/precipitation transition. . This step increase in Rd could however also be interpreted as being a consequence of using batch experiments. Indeed, since AFm has a very fast equilibration kinetics, equilibrium Al and Ca concentration are reached in batch experiments very fast (Marty et al., 2018). The combination of high Al and Ca concentration together with increasingly higher concentration of MoO_4^{-2} in solution could induce, once a given MoO_4^{-2} concentration exceeded, dissolution of pristine AFm and precipitation of the AFm-MoO_4^{2-}. However, this hypothesis requires further validation. This shows the very high degree of complexity that is inherent to the study of such cement phases.

Ma et al. (2018) have shown that is a relationship between surface edge area and sorption site density for MoO_4^{-2} sorption indicating edges as sorption sites. However, no such relation can be established in the case of SeO_3^{-2} sorption, suggesting that SeO_3^{2-} adsorption is not only taking place on surface edge sites. They observed outer sphere configuration of adsorbed Se(IV) for Se concentrations lower than those necessary for AFm-SeO_3^{-2} formation.

The retention of radionuclides by cementitious materials can also be quantified by a solid liquid distribution ratio, R_d, defined as

$$R_d(RN)\ [L\cdot kg^{-1}] = \frac{\{RN\}}{[RN]} \quad (1)$$

with {RN} the concentration of radionuclide sorbed on the solid (mol/kg) and [RN] the radionuclide concentration in solution (M).

The R_d value only describes the distribution of a radionuclide between the solid phase and the liquid pore solution and does not imply any mechanistic process. Sorption constants were measured for a large suite of individual cementitious phases and various HCP. In some cases more than one laboratory has obtained R_d values for the same phase and radionuclide, allowing direct comparison.

MoO_4^{2-}

The interaction of molybdenum with cementitious materials has received relatively little attention to date. In early studies at high Mo concentrations (Kindness et al., 1994), formation of $CaMoO_4$ generally prevented uptake

by cementitious phases. Those R_d values were obtained at initial Mo concentrations low enough to avoid powellite formation ranged between 30 and 100 L·kg^{-1}. Zhang and Reardon (2003) studied the incorporation of molybdate by hydrocalumite and ettringite using lower concentrations of molybdate. Ettringite showed an anion preference in the order $B(OH)_4^-$ > SeO_4^{-2} > CrO_4^{-2} > MoO_4^{-2}.

In the present work, molybdate uptake on C-S-H phases and its dependency on the Ca/Si ratio were studied by two different laboratories. Both found a higher distribution ratio for high Ca/Si ratios (Figure 5). These findings are in agreement with the change in surface charge of C-S-H to positive values at Ca/Si ratios exceeding 1.2 (Churakov et al., 2014), suggesting electrostatic sorption of the molybdate anion on C-S-H. In fact, R_d values for C-S-H1.4 (R_d ~780 vs. 20 L kg^{-1}) were much higher than for C-S-H0.9 or C-S-H 0.8 (R_d ~430 vs. 4 L·kg^{-1}), although, partly due to differences in specific surface area, significant differences in the R_d value occurred between the measurements of two different laboratories. These results show that C-S-H phases in cementitious materials can play an important role with respect to the retention of molybdenum, in particular in aged systems (stage II and III).

Much lower R_d values for molybdate sorption were observed in alkali-rich, young cementitious water (pH 13.5), probably due to competition with OH^- species for sorption sites on the C-S-H or to the negative zeta potential of CSH phases reported for pH 13.5 (Pointeau et al., 2006).

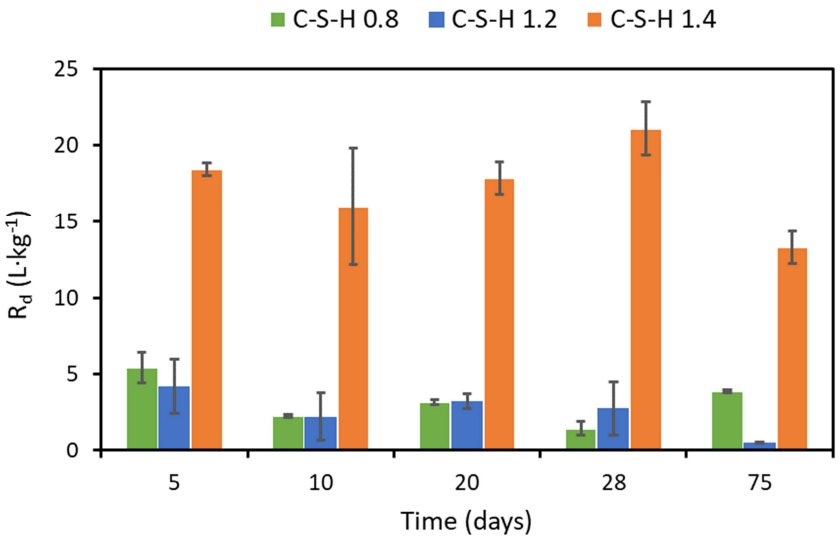

Figure 5: Dependency of MoO_4^{2-} retention on C-S-H phases as function of the Ca/Si ratio and time (Mo initial concentration 10^{-6} M) (for experimental conditions see supplementary materials 3.1 and 3.2).

Pronounced molybdate uptake (R_d ~1500 L·kg^{-1}) by **AFm-SO_4** and **AFm-CO_3** was observed by two independent laboratories suggesting no preferential uptake results from the nature of the interlayer anion (i.e. planar CO_3^{-2} or tetrahedral SO_4^{-2}). XRD studies on the AFm-SO_4^{-2} used in the batch sorption experiments showed an increase in the basal spacing compared to pure AFm-SO_4^{-2}, indicating structural incorporation of MoO_4^{-2}-ions in the AFm-structure by anion exchange with the interlayer anion, since the size of the molybdate oxo-anions (Mo-O bond length ~1.77 Å) is larger than that of SO_4^{-2}-ions (S-O bond length ~1.47 Å).

Less definitive information was obtained for adsorption of MoO_4^{-2} on AFt. Uncertainties are between 122 L·kg^{-1} and 3 L·kg^{-1}, the latter value being similar to that given by Ochs et al. (2016) is considered too high (Table 2).

Molybdate sorption has also been studied in **AFm/AFt mixtures**. Low molybdate retention was observed in samples of S(VI)/Al equal to 2 and 2.5 where AFt is the major component. In contrast to the study of (Pointeau et al., 2006) of AFt suspensions in DDW or porewater from fresh HCP, in our study, the surface of AFt solids is expected at the observed pH of about 11.6 to have very low zeta potential, which turn negative in the presence of sulphate anions (Zingg et al., 2008) at sulphate concentrations such as those observed in our study (as high as 55

mM) and hence, may hinder the retention of anionic species as molybdate. In contrast, strong molybdate retention occurs in the samples of S(VI)/Al equal to 1 and 0.5 where AFm is the major component, with values ranging from 164<R_d<693 L·kg^{-1}. The highest R_d was observed in samples without ettringite (S(VI)/Al = 0.5) with values ranging from 1200 to 46400 L·kg^{-1}. This suggests that a revision of the literature, linking high retention of molybdate to presence of ettringite, is necessary (Ochs et al., 2016).

The high molybdate uptake by **hydrogarnet** (R_d 3000 L·kg^{-1}) was found to be due to the neo-formation of a molybdenum bearing AFm-like phase, which can also become a pure AFm-MoO_4^{-2} phase or a mixture of this phase with the Mo-analogue of the so called U-phase, depending on pH and alkali concentrations in solution. Hydrogarnet has also been identified (Hillier et al., 2007) as a major phase in chromium ore processing residue and has a capacity to host homologue CrO_4^{-2}.

I^-, IO_3^-

Several publications in the literature provide indications that ettringite and AFm phases exhibit good I^- and IO_3^- retention properties. Mattigod et al. (2001) observed a reduction of the leachability of iodine in a cement-based materials containing steel fibres due to the reduction of IO_3^- to I^-. Iodide sorption onto cement has been shown to increase with increasing Ca/Si ratios in C-S-H gels in spite of an increased competition from OH^- at sorption sites, suggesting I^- is sorbed electrostatically (Glasser et al., 1989; Pointeau et al., 2008).

Aimoz et al. (2012) showed that I^- uptake strongly depends on the anion originally present in the AFm interlayer. No I^- uptake was observed in the case of AFm-CO_3 and AFm-Cl_2. Only AFm-SO_4 was found to take up considerable amounts of I^- in its interlayer. This observation is in excellent agreement with the solid solution studies described above and in (L. Nedyalkova et al., 2019) showing the existence of a miscibility gap in the composition range 0.5 ≤ $CO_3^{-2}/(2I^-+CO_3^{-2})$ indicating that small amounts of I^- cannot mix with the CO_3^{2-} anions present in the interlayer of AFm-CO_3.

The present work confirmed this dependence of the I^- uptake on the original interlayer occupancy. Structural incorporation of iodide (I^-) by anion exchange in the interlayer was observed for **AFm-SO_4^{-2}** (R_d ~811±324 L·kg^{-1} at pH 12 and R_d ~30±5 L·kg^{-1} at pH 13) and **AFm-CO_3^{-2}** (R_d ~81±32 L·kg^{-1}). The observed decrease of Rd with increasing pH corresponds well to the data of Atkins and Glasser (1992). The uptake of iodate (IO_3^-) by **AFt** as well as by **AFm-SO_4^{-2}** was shown to lead to iodate-substituted ettringite, formed either by anion exchange or by phase transformation.

The increased uptake of iodide in **C-S-H** with increasing Ca/Si-ratio reflects increasing positive surface charge at high Ca/Si, as anticipated from the assumed electrostatic adsorption mechanism for iodide on C-S-H, although iodide uptake by C-S-H is generally lower (R_d 40 - 80 L·kg^{-1}) than on AFm/t or hydrogarnet. In general, all model phases showed a higher uptake for iodide and iodate in artificial young cement water when compared to the equilibrium solutions. The results of experiments exploring iodide and iodate adsorption on crushed HCP based on **CEM I** revealed a fast uptake of both oxidation states, with slightly lower sorption of iodine (R_d ~25 L·kg^{-1}) than iodate (R_d ~140 L·kg^{-1}), in good agreement with existing literature data, (e.g. Bonhoure et al., 2002, Pointeau et al., 2008). Overall, the results obtained for the uptake of iodide and iodate by HCP systems are in qualitative agreement with results obtained for the single hydration phases under equilibrium conditions, indicating that at least for the low iodine concentrations expected under repository conditions, the major contribution to iodine uptake can be attributed to minor cement hydration phases such as AFm/AFt.

TcO_4^-

Allen, et al. (1997) demonstrated that the addition of blast furnace slag (BFS) to a cement formulation leads to partial reduction of any pertechnetate anions present, whereas the addition of Na_2S or FeS results in complete reduction to the less mobile Tc(IV). Berner (1999) suggested that binding and/or incorporation of TcO_4^- into the alumina ferric mono/tri-sulphate (AFm/AFt) phases of cement systems could also be expected, by analogy to other oxo-anions such as SO_4^{-2} or MoO_4^{-2} , and possibly also SeO_3^{-2}. Moreover, several minerals are known to

incorporate technetium, for example fougerite (green rust), a layered double hydroxide ($[Fe^{2+}_4Fe^{3+}_2(OH)_{12}][CO_3^{-2}]\cdot 3H_2O$) and potassium metal sulphides. A good overview of potential host phases is given by Luksic et al. (2015).

In the present work, the uptake of pertechnetate (TcO_4^-) by the individual cementitious phases investigated was found to be generally low (Table 2), suggesting that reductants such as Fe(II) and/or Fe(II)-containing phases, which were not studied here, may play a key role in technetium retention in certain cementitious system. These experiments elucidated the high mobility and low retention of TcO_4^- in cementitious environments in the absence of reductants. The possible uptake of TcO_4^- by AFm/AFt, which was suggested for example by Berner (1999), as a potential retention mechanism, was found to be weak; R_d < 1 $L\cdot kg^{-1}$, indicating practically no uptake due to exchange for SO_4^{-2}-groups. Batch-uptake experiments on crushed HCP were performed in order to study the potential accumulation of reduced Tc on reductive sites such as Fe(II)-bearing phases originating from BFS. The uptake experiments conducted for more than 75 days, revealed only minor uptake of TcO_4^- by HCP. As expected considering the lower content of Fe(II) and/or sulphides, the distribution ratios of HCP based on CEM I tend to be lower (R_d ~2 $L\cdot kg^{-1}$) than those obtained for CEBAMA low-pH paste (R_d ~9 $L\cdot kg^{-1}$).

$^{14}CO_3^{-2}$

Inorganic carbon-14 sorption by cementitious materials can be considered in terms of two porcesses (Evans, 2008): (i) electrostatic adsorption onto a positively charged site and (ii) precipitation. Adsorption for inorganic carbon ($^{14}CO_3^{-2}$) occurs only when carbonate levels are well below the threshold at which calcite precipitation starts (about 1-2x10^{-5} $mol\cdot L^{-1}$). Isotopic exchange with solid $CaCO_3$ present in HCP controls the $^{14}CO_3^{-2}$ retention in HCP (Bradbury and Sarrot, 1995) but the extent of removal of $^{14}CO_3^{2-}$ is very dependent on the particular cement system in question. Results obtained from batch sorption experiments and zeta potential measurements (Noshita et al., 1995) suggest that the adsorption mechanism for $^{14}CO_3^{-2}$ onto cationic surfaces of C-S-H phases at high Ca/Si ratio (-$SiOCa^+$) is electrostatic adsorption.

Adsorption experiments were conducted on both fresh and degraded cement pastes (experimental conditions and definition of degradation states: Supplementary material 1 and 2). The degradation stages III.a to IV describe the C-S-H evolution from C-S-H 1.3 (stage III.a) to C-S-H 0.7 (stage IV), all corresponding to the denotation of cement degradation I, II, III, IV given by Ochs et al. (2016). The kinetic tests carried out showed that equilibrium was achieved for all cement pastes based on CEM I and CEM V after ~40 days. At equilibrium, more than 80% of the initial ^{14}C present in the contacting solution was adsorbed onto non-degraded CEM I as well as onto the first two degraded pastes (stage III.a and stage III.b), but only ~ 30% was adsorbed on the most degraded cement paste (stage IV). Thus, the $^{14}CO_3^{-2}$distribution ratio is greatly affected by the extent of cement degradation, with values ranging between 1600±268 L/kg for stage I cement paste, to 120±36 L/kg for stage IV. $^{14}CO_3^{-2}$ uptake on CEM V is significantly higher than on CEM I cement paste (3500±275 $L\cdot kg^{-1}$). The experimental data indicate that ^{14}C adsorption is not attributable solely to isotopic exchange and that precipitation of ^{14}C containing calcite cannot be excluded. This could explain the results of desorption tests (carried out for non-degraded CEM I and on the most degraded paste, stage IV) which indicate that desorption equilibrium is attained after a slightly longer time than sorption equilibrium (~ 60 days) at which point around 80% of the ^{14}C originally adsorbed was released back to solution.

The effect of carbonation of CEM V samples on $^{14}CO_3^{-2}$ uptake and the degree of reversibility of the sorption/desorption process are shown in Figures 6 a and b.

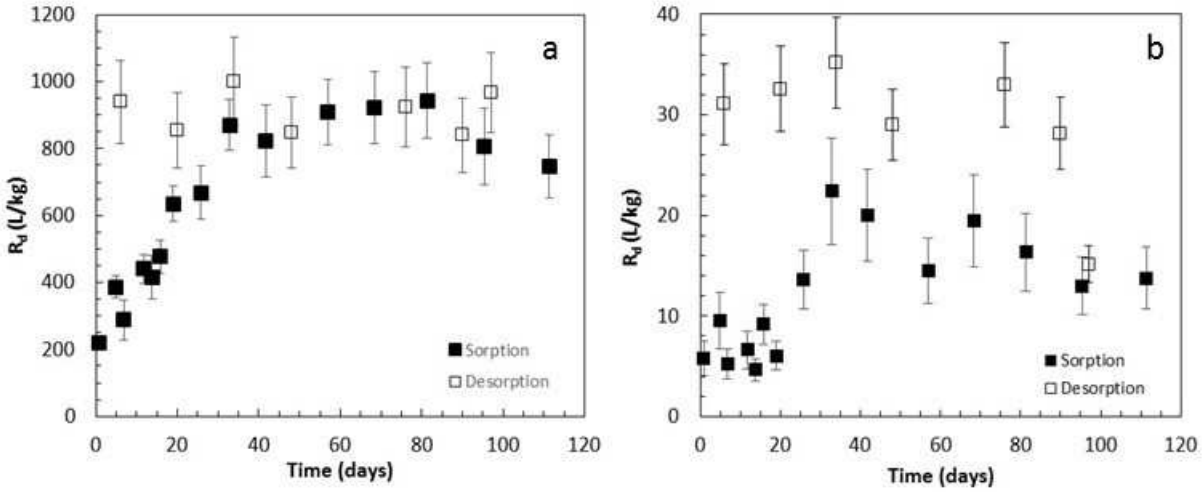

Figure 6: Evolution of ^{14}C distribution ratios (R_d) vs time on non-carbonated (Fig. a) and carbonated CEM V (Fig. b). Initial ^{14}C concentration is 6 10^{-8} mol.L^{-1}

For non-carbonated CEM V (state I), the steady-state is reached after around 60 days. The corresponding R_d value is 800 ±100 L·kg^{-1} for a pH of 13.5, much lower than the value of 3200 L·kg^{-1} obtained at pH 12.5 (Fig. 6 a). The magnitude of the Rd values measured and their dependency on pH are in close agreement with the data obtained by Pointeau et al. (2008) for CEM I HCP at pH=12.5 (5000 L·kg^{-1}) and pH=13.2 (500 L·kg^{-1}).

The desorption experiments show that the uptake process at trace level seems to be reversible. In contrast, for ^{14}C concentrations above the solubility limit of calcite ($5\cdot10^{-6}$-$5\cdot10^{-4}$ mol.L^{-1}), ^{14}C uptake was found to be irreversible ($Rd_{desorption}$>$Rd_{sorption}$ by one order of magnitude). For non-carbonated HCP, ^{14}C can be either adsorbed on C-S-H or exchanged on the "residual" calcite (always present as dispersed particles in cement paste at ~ 5% in mass).

For carbonated CEM V HCP (state IV), steady-state is reached after 40-50 days and the corresponding R_d value is 20±5 L·kg^{-}1. Due to the predominance of calcium carbonates in these samples, this Rd value can directly be compared to Pointeau et al's value (cited in Henocq et al., 2018) obtained on calcite in 0.1 mol.L^{-1} NaOH solution (R_d= 10-20 L·kg^{-1}). As noted above, $Rd_{desorption}$ values of 30±5 L·kg^{-1} are slightly higher than $Rd_{sorption}$ values. In this case, the partial irreversibility could be consistent with the uptake of ^{14}C on calcite by a two-step mechanism (isotopic exchange and subsequent incorporation by diffusion in calcite).

SeO_4^{-2} and SeO_3^{-2}

Under the alkaline reducing conditions expected in a cementitious near-field, Se(IV), Se(0) and Se(-II) are expected to be the predominant redox states and aqueous Se speciation dominated by the anionic species SeO_3^{-2}, HSe^- and a series of polyselenides (Se_x^{-2}), mainly Se_2^{-2}, Se_3^{-2} and Se_4^{-2}. Relatively few studies have focused on the solubility of selenium under high pH conditions. Baur and Johnson (2003) and Ma et al. (2018) found experimental evidence for the formation of $CaSeO_3\cdot H_2O$ as solubility controlling Se(IV) phase in their Se(IV) sorption studies onto AFm phases. These authors could reproduce their Se(IV) sorption data onto AFm phases only assuming $CaSeO_3\cdot H_2O$ precipitation at high loadings applying apparent log K_{s0} values of -7.29 to -7.27. These values are more than half an order of magnitude lower than the log K_{s0} value for $CaSeO_3\cdot H_2O$(s) reported in most selenium thermodynamic databases (e.g. Hummel et al., 2002b).

Felipe-Sotelo et al. (2016) observed on the other hand the formation of $Ca_2SeO_3(OH)_2\cdot 2H_2O$ as the solubility limiting phase in 95%-saturated $Ca(OH)_2$ and NRVB (Nirex Reference Vault Backfill)-equilibrated solutions whereas Solem-Tishmack et al. (1995) indicating that selenite could be retained as 'selenite-ettringite' in sulphate-rich cement admixtures. Mace et al. (2007) suggest that ettringite could play an important role in the retention of Se(IV) at higher temperatures (70°C). Calcite may also contribute to the retention of selenite and other oxyanions in alkaline conditions (Cornelis et al., 2008). Johnson et al. (2000) investigated the adsorption of SeO_3^{-2} onto 27 cement formulations. They found that the water to cement ratio during curing and the clay content of the cement

mix had no influence on the selenite uptake. Increasing silica fume contents, however, decreased the selenite uptake probably caused by decreasing Ca/Si ratios of the C-S-H phases resulting in a negative surface charge and thus in lower anion sorption.

Baur and Johnson (2003) carried out batch studies on the uptake of SeO_3^{-2} by individual cement phases, namely ettringite, monosulphate and C-S-H; they postulated that binding of SeO_3^{-2} occurs mainly on mineral surfaces owing to surface complexation and surface precipitation with calcium. This hypothesis is supported by extended X-ray absorption fine structure (EXAFS) experiments carried out by Bonhoure et al. (2006) where SeO_3^{-2} bound to the cement appears to show non-specific interaction with the cement minerals, whether C-S-H, portlandite, ettringite or monosulphate. Moderately strong uptake of Se(IV) was observed in these studies on main cement phases with R_d values of 180 $L \cdot kg^{-1}$, 380 $L \cdot kg^{-1}$ and 210 $L \cdot kg^{-1}$ on ettringite, C-S-H phases and AFm phases, respectively. Some association between calcium and selenium is a common observation in the majority of the investigations.

In the present work, the retention of selenium species ($Se^{IV}O_3^{-2}$/$Se^{VI}O_4^{-2}$) was shown to be due to uptake by AFm phases and to a lesser degree, AFt, which all showed a tendency for higher uptake of the more oxidised selenium species. Moreover, a distinctively stronger retention of both Se-species by AFm-SO_4 compared to AFm-CO_3^{-2} was observed, indicating a dependency on the interlayer anion. In comparison to the aluminate phases, the uptake of selenium on C-S-H was found to be comparatively low (R_d $Se^{IV}O_3^{-2}$: ~100 L kg^{-1}; R_d $Se^{VI}O_4^{-2}$: ~10 L kg^{-1}). Due to the higher proportion of aluminate phases in HCP based on CEM I, the retention capacity for selenite and selenate is higher than on the low–pH CEBAMA reference paste; remarkably, in all cases, the HCP showed higher R_d values for $Se^{IV}O_3^{-2}$ than for $Se^{VI}O_4^{-2}$. Retention values for all systems studied are given in Table 2.

$Be(OH)_3^-$ and $Be(OH)_4^{-2}$

No experimental investigations of Be(II) uptake by cement and cementitious minerals are available in the literature. Due to the lack of experimental data and the predominance of negatively charged hydrolysis species $Be(OH)_3^-$ and $Be(OH)_4^{-2}$ in the pore water conditions expected in cement systems, some review studies conservatively proposed a R_d = 0 for this system (Wieland and Van Loon, 2003, Ochs et al., 2016).

Figure 7 shows the main results obtained in the present study (experimental data: see supplementary data, 4) for the uptake of Be(II) by standard and low pH cement (CEM I 42,5 N BV/SR/LA and CEM I 42,5 MH/SR/LA, respectively) and C-S-H phases with Ca/Si = 1.0 and 1.6. The data points shown in the figure represent average log R_d values for systems with Be concentration below the solubility limit for the corresponding pH. A very strong uptake of beryllium by cement and C-S-H phases is observed in all investigated systems. The figure shows a trend to decrease $\log_{10} R_d$ with increasing pH, with the highest $\log_{10} R_d$ values observed for low pH cement with pH ≈ 11.4, and the lowest for CEM I in degradation stage I (pH ≈ 13). A good agreement is obtained between $\log_{10} R_d$ values obtained for C-S-H with Ca/Si = 1.6 and CEM I in degradation stage II. This is in line with the predominance of C-S-H phases with Ca/Si = 1.6 in degradation stage II of standard Portland cement (pH ≈ 12.5).

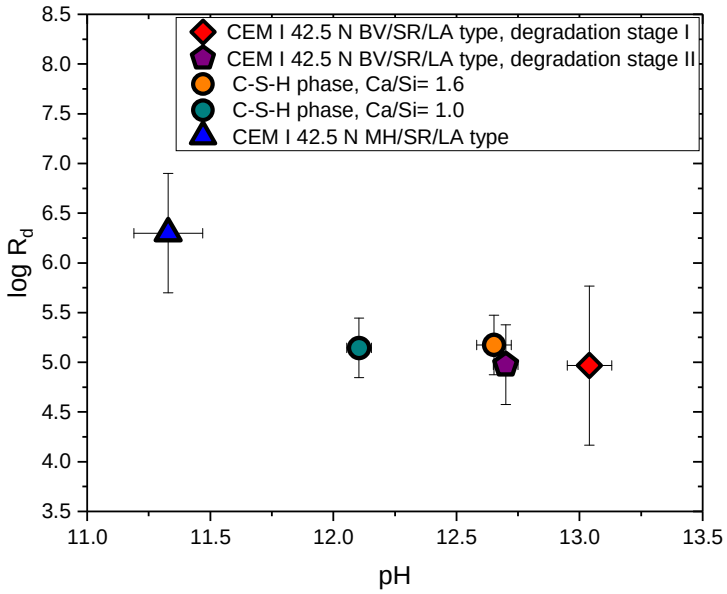

Figure 7: *Uptake of Be(II) by cement (CEM I 42,5 N BV/SR/LA type, degradation stages I and II) and C-S-H phases with Ca/Si = 0.6, 1.0 and 1.6. R_d values provided in L·kg^{-1}.*

Ra^{+2}

Experimental data on radium sorption on cementitious materials are scarce. (Tits et al., 2006a) investigated the interaction of Ra with C-S-H and hydrated cement pastes. For fresh HCP a two-step process could explain the Ra(II) uptake: fast sorption within one day (R_d value of 260 L·kg^{-1}), followed by a slowly increase of Ra (II) uptake towards equilibrium over a period of 60 days (to an R_d value of 400 L·kg^{-1}). This may be compared to the very fast uptake of degraded HCP, which reaches equilibrium within one day at a R_d of 140 L·kg^{-1}. There is good evidence that Ra^{+2} sorption increases as the Ca/Si ratio decreases on C-S-H. It is assumed that Ra(II) only sorbs on the C-S-H fraction in HCP and that the aqueous Ra(II) speciation is dominated by the Ra^{+2} species. The maximum distribution ratio was reported by (Tits et al., 2006a) for C-S-H with Ca/Si = 0.96, approx. 4×10^3 L·kg^{-1}, and decreased to approx. 1.5×10^2 L·kg^{-1} for C-S-H with Ca/Si = 1.6. Tits et al. (2006a) also investigated the desorption of radium from the above mentioned phases and observed that radium sorption onto C-S-H phases is linear and reversible.

In the frame of CEBAMA, the uptake of Ra2+ by both, HCP and various hydrated cement phases, including C-S-H, AFm/Aft, hydrogarnet and portlandite, was studied. The results revealed a fast Ra uptake by the various hydration phases leading to sorption equilibrium within 10 to 28 days. **C-S-H** was the only investigated phase showing a significant uptake of ^{226}Ra, whereas the uptake of ^{226}Ra in systems with AFt and AFm phases was found to be significantly lower (Lange et al., 2018). A distinct dependence of the ^{226}Ra uptake by C-S-H on the Ca/Si ratio and solution composition was confirmed, decreasing from about 22000 L·kg^{-1} (C-S-H0.9) to 1800 L·kg^{-1} (C-S-H1.4) in alkali-free systems. This effect is probably due to the negative surface charge at Ca/Si <1.2, facilitating cation uptake, as well as to the higher competition with Ca ions in solution for sorption sites at high Ca/Si ratios. The measured R_d values are however higher than those reported by Tits et al. (2006a) but consistent to recent observations of Olmeda et al. (2019). R_d values were about a factor of 2 lower in systems with artificial young cementitious water (pH 13.5) due to competition with alkalis for sorption sites, as well as changes in C-S-H surface charge and speciation at higher pH. The results suggest a stronger retention and lower mobility of ^{226}Ra in alkali-poor, aged cementitious systems at stage II (portlandite stage) compared to young cementitious materials in stage I. Moreover, the lower Ca/Si ratios of C-S-H in cementitious materials prepared from low pH cements – as well as partly decalcified C-S-H during stage III – should provide for a higher retention capacity for ^{226}Ra than C-S-H in young OPC based systems.

The uptake of ^{226}Ra by C-S-H is generally explained in terms of cation exchange with calcium and sorption to two silanol-like sites at the C-S-H surface. Assuming Ra exchange for Ca as the main uptake mechanism (cf. Tits et al., 2006a), selectivity coefficients for the exchange reaction

$$\text{C-S-H-(Ca)} + Ra^{2+} \leftrightarrow \text{C-S-H-(Ra)} + Ca^{2+}$$

where C-S-H-(Ca) refers to the exchangeable Ca in the C-S-H structure, were calculated from the R_d-values and Ca-concentrations obtained in the sorption experiments. The selectivity coefficient, K_c, for this reaction is defined as:

$$K_c = \frac{N_{Ra} \cdot \mathrm{a}(Ca^{2+})}{N_{Ca} \cdot \mathrm{a}(Ra^{2+})}$$

where $a(Ca^{2+})$ and $a(Ra^{2+})$ are the ion activities in the aqueous phase and N_{Ra} and N_{Ca} refer to the equivalent fractional occupancies:

$$N_{\mathrm{M}} = \frac{2 \cdot \{M_s^{2+}\}}{CEC}$$

with $\{M_s^{2+}\}$ as the amount of the respective divalent cation sorbed (mol kg^{-1}), and *CEC* the cation exchange capacity of the C-S-H phase in eq kg^{-1}. For homovalent cation exchange, the activity coefficients for both cations are identical; thus the activities can be substituted by concentrations, leading to:

$$K_{\mathrm{c}} = \frac{N_{\mathrm{Ra}} \cdot [Ca^{2+}]}{N_{\mathrm{Ca}} \cdot [Ra^{2+}]}$$

Attributing the Ra uptake only to cation exchange, the relation between the selectivity coefficient for the Ra-Ca exchange and the distribution coefficient R_d of Ra can be calculated as:

$$R_{\mathrm{d}} = \frac{0.5 \cdot CEC \cdot K_{\mathrm{c}}}{[Ca^{2+}]}$$

Based on this, we obtained selectivity coefficients for the Ra/Ca exchange in the alkali free systems of log K_c = 2.2 for C-S-H0.9 and log K_c = 1.8 for C-S-H1.4 (Lange et al., 2018). These values are much higher than the values given by Tits et al. (2006a) log K_c(Ra-Ca) = 0.77, independent of the Ca/Si ratio. No explanation is yet available for this inconsistency. The comparison with data for other alkaline-earth elements reveals a decreasing affinity for uptake by C-S-H in the order $Ra^{+2} > Ba^{+2} > Sr^{+2}$ (Ba^{+2}: log K_c=1.05,(Missana et al., 2017); Sr^{+2}: log K_c=0.08, (Tits et al., 2006b)). Sr^{+2} is not a meaningful analogue for the uptake of ^{226}Ra in cementitious systems due to the significantly lower selectivity coefficient.

The uptake of $^{226}Ra^{+2}$ by HCP prepared from CEM I reached a steady state after about 10 days with an R_d value of ~60 L kg^{-1}. In contrast, in the sorption experiments using the low pH (Cebama reference blend) HCP, equilibrium conditions were not attained in 100 days, which, in combination with the changes in solution pH, suggested an ongoing hydration process in this material and the formation of C-S-H with low Ca/Si-ratios from remaining unreacted clinker phases, silica fume and blast furnace slag. The final R_d value of 12,300 L kg^{-1} is attributed to both, the lower system pH and the lower Ca/Si ratio of the C-S-H compared to CEM I based systems.

The results from the kinetic sorption tests (supplementary data, 1.1) on degraded and non-degraded CEM I and CEM V HCP indicate that most of the $^{226}Ra^{+2}$ was sorbed mostly in the first 2 days of contact (sorption percentage ~ 33% for CEM I and 35% for CEM V). After two days, radium uptake slowly increase up to 20 days for both cement pastes, up to an distribution ratio of ~300 L·kg^{-1} for CEM I and ~400 L·kg^{-1} for CEM V (Figure 8). No significant increase was observed in radium uptake between 20 and 80 days of contact, indicating that 20 days of contact are enough to attain the sorption equilibrium.

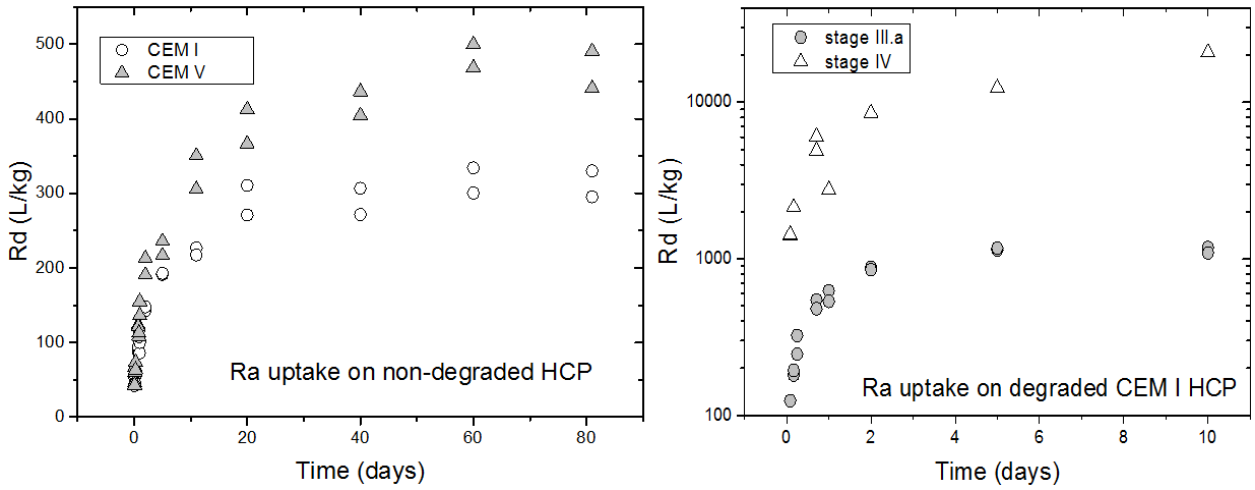

Figure 8: Comparison of Ra uptake on non-degraded CEM I and CEM V (left Fig.) and the effect of degradation on uptake on CEM I (right Fig.).

For degraded HCP (stage III.a and stageIV) the Ra uptake is faster than for non-degraded pastes. The radium uptake on these two degraded pastes is significantly higher than on the non-degraded one (~ 1000 $L \cdot kg^{-1}$ for stage III.a and ~ 20000 $L \cdot kg^{-1}$ for stage IV of degradation, Figure 8 right). Sorption isotherms were linear between 45 $Bq \cdot ml^{-1}$ and 136 $Bq \cdot ml^{-1}$ ($5.4 \cdot 10^{-9}$ to $1.6 \cdot 10^{-8}$ mol/L) for non-degraded and degraded ones samples.

The reversibility of radium sorption on non-degraded cement pastes was assessed by desorption tests. Radium desorption is much slower than sorption. After 20 days, only about 40% of sorbed Ra was desorbed from CEM I and ~20% from CEM V and even after 80 days less than 50% is desorbed from both cement pastes.

The temperature dependency was studied for Ra uptake on CEM II/A-S 42.5 R both in saturated $Ca(OH)_2$ and synthetic cement water CPW (Table 1) and in Concrete Richard (containing cement of CEM III B/32.5 type) and Concrete UJV (with cement of CEM I 42.5 type).

Table 1: Distribution coefficients R_d [$L \cdot kg^{-1}$] for Ra sorption on cement based materials as a function of temperature. R_d values are averages obtained for liquid to solid ratio of 10, 60 and 100 $L \cdot kg^{-1}$

	HCP CEM II/A-S 42.5 R, $Ca(OH)_2$				CEM II / B-M (S-LL) 32.5R	Concrete UJV/ $Ca(OH)_2$	Concrete Richard/ $Ca(OH)_2$
	22 °C	50 °C	65 °C	80 °C	22 °C	22 °C	22 °C
R_d [$L \cdot kg^{-1}$]	93±21	121±11	213±72	275±169	352±154	179±47	166±65

At room temperature, the R_d increased in the order: hydrated cement paste CEM II/A-S 42.5 R < concrete Richard <concrete UJV in saturated $Ca(OH)_2$ solution, despite the lower content of cement and hence of C-S-H in concrete. Interesting were the resulting R_d for CEM II - B-M (S-LL) 32.5 R. However, both CEM II materials differ in the value of specific surface area (2.4 times higher for CEM II-B-M (S-LL)32.5 R)) and also different liquid phases were used for the sorption experiments.

In order to assess some general tendencies, a comparison for sorption constants is given in Table 2. The sorption constants in this Table show same variability depending on the measurement conditions used in the different laboratories including S/L ratio, specific surface area and total concentration of the element whose sorption is tested. In general, the anions MoO_4^{2-}, SeO_3^{2-}, SeO_4^{2-}, TcO_4^-, I^-, IO_3^-,and Cl^- were bound preferentially on AFm and AFt phases while the uptake on C-S-H was weaker, but still relevant. AFm and AFt phases sorb preferentially the

divalent anions (MoO_4^{2-}, SeO_3^{2-} and SeO_4^{2-}) over monovalent anions such as TcO_4^-, I-, IO_3^-, and Cl^-. The cation Ra^{2+} is preferentially bound on C-S-H; its uptake on AFm phases is much weaker. The sorption measured on cement pastes shows a large variability due to the complexity of cementitious systems and due to the presence of high concentrations of competing anions such as sulfate in the solution. The table show clearly higher Rd values for the uptake of Be(II) than Ra(II). Although both elements belong to the alkali-earth series, they are characterized by very different ionic radii (rBe2+ = 0.27 Å for coordination number (CN) = 4; rRa2+ = 1.48 Å for CN = 8). This results also in a very different hydrolysis behaviour (strong hydrolysis for Be(II) against weak hydrolysis for Ra(II)), which is expectedly the main reason for the observed differences in the uptake by C-S-H phases."

Table 2: Comparison of sorption constants Rd [$L \cdot kg^{-1}$] obtained by the various laboratories in the CEBAMA project (P=PSI/EMPA, J=Jülich, B=BRGM, A=Amphos21, R=RATEN, K=KIT, S=SUBATECH, C=CTU). Data for Be are: 10^{-6} M ≤ [Be(II)]0 ≤ $10^{-2.5}$ M (depending upon Ca:Si of C-S-H and Be(II) solubility limit at the investigated pH) and [S/L] = 2 g·L-1. For Ra: initial concentrations are $5.5 \cdot 10^{-9}$ M (pH 12.5) and S/L is 2.5 $g \cdot L^{-1}$ for CEM I and V for RATEN. For C14 sorption initial concentrations are 10^{-7} M (CEMI) and $3 \cdot 10^{-8}$ (CEMV) S/L= 2.5 $g \cdot L^{-1}$ and pH 12.5 for RATEN.

	I	IO3	Se(VI)	Se(IV)	C-14	Ra	Be	TcO4-	MoO4
AFm-SO4	30±5 (P) pH13 811±324 (J) pH 12	634±253 (J) pH 12	92±18 (P) pH13 9836±1680 (J) pH12	718 ±144 (P) pH13 4430±538(J) pH12		7±4.3(J)		4.0±1.9(J)	1500 (B) 1571±115(J) pH12
AFm-CO3	81±32 (J) pH 11.3	51±20 (J)	5±1 (P) pH13 120±36(J) pH 11.3	47±10(J) pH11.3		4±3.9(J)		2.3±1.7(J)	1500 (B) 1564±90(J) pH 11.3
Afm-CO3-OH	55±10 (P)		935 ±187 (P)						
Afm/Aft S(VI)/Al=0.5									1200-46000 (A)
Afm/Aft S(VI)/Al=1									160-170 (A)
AFt	190±76 (J)	1068±427 (J)	728±90 (J)	97±4 (J)		139±28 (J) (precipit?)		0.6±0.9(J)	<<3 (A) 122±4(J) pH 11.2
Hydrogarnet									3000 (J)
CSH 1.4±0.2	83±33 (J)	62±24 (J)				1805±772 (J)	150000 (K)	2.3±2.4(J)	20±5(A) pH 12.3 781±41 (J)
CSH 0.8±0.2	48±19 (J)	64±25 (J)	13±1 (J)	124±20(J)		22530 ±3980 (J)	150000 (K)	4.5±2.7(J)	4±2 (A) pH 10.3 432±26 (J)
CEM I	25 (J)	140 (J)			1300 (R)	300 (R) 60 (J)			
CEM II						130 (C) S/L>0.01			
CEM V					3200 (R) pH 12.4 800 (S) pH 13.5	500 (R)			
CEBAMA mix						12600 (J)			

Diffusion of Cl^-, I^-, TcO_4^-, HTO, $^{14}CO_3^{-2}$, Sr^{+2} and Ra^{+2} in HCP

Diffusion of ^{36}Cl- through Nirex Reference Vault Backfill (a candidate cementitious backfill material) has been investigated by van Es et al. (2015), who reported significant retardation of ^{36}Cl in NRVB. Moreover, the data displayed a pronounced dependence on the background chloride concentration, whereby trace ^{36}Cl retention was substantially reduced in saline solutions. Autoradiographic and elemental mapping by energy-dispersive X-ray spectroscopy (EDX) suggested that ^{36}Cl is bound to partially hydrated, glassy, sulphate-bearing, residual clinker particles. In this work, the PFA blend showed the lowest retention for $^{36}Cl^-$ with recovery reaching 90% of the input concentration after 270 days (Fig. 9). . On the basis of this result, the diffusion of chloride through PFA:OPC

could be assumed conservatively, to correspond to that of HTO. In contrast, no breakthrough was observed for ^{36}Cl with CEM I. Whether binding to clinker can account for the retardation, as suggested for NRVB (van Es et al., 2015), is by no means certain since there has clearly been some diffusion from the central well and this appears to be homogeneous, as shown by the accompanying autoradiograph (Fig 9).

A number of studies have been carried out investigating the through-diffusion (Atkinson and Nickerson, 1984, Sarott et al., 1992, Felipe-Sotelo et al., 2014) and out-diffusion (Mattigod et al., 2001) of I^-. The rate of I^- diffusion has been shown to correlate strongly with the water to cement ratio of the paste where an increase from 0.2 to 0.7 can increase the diffusion rate by three orders of magnitude (Atkinson and Nickerson, 1984). This work would seem to corroborate these findings as markedly different diffusion behaviour was observed for the respective cement formulations (Fig. 9). The breakthrough curves for iodide and tritiated water in PFA:OPC are similar in terms of both earliest appearance of the tracer at the first sampling point (1 day) and overall recovery (C/C_0 > 80%). Thus, as a first and conservative approximation, the diffusion coefficient for iodide through this particular cement could be assumed to be the same as for HTO. Conversely, I^- is effectively retarded by CEM I with no breakthrough observed on the timescale of the experiment and therefore, no reliable diffusion rate can be inferred. The remaining cements studied all displayed a greater capacity for retarding iodide migration than chloride but detailed discussion is beyond the scope of this paper.

No comparable data for ^{99}Tc are available in the literature but analogous experiments to those described above (Felipe-Sotelo et al., 2014; van Es et al., 2015) were carried out for various HCP samples, including NRVB. Selected breakthrough curves highlight the differential transport of $^{99}TcO_4^-$ in NRVB, PFA and CEM I (Fig. 9c). **$^{99}TcO_4^-$** was observed to migrate through each of the cements, albeit at different rates. For PFA:OPC, the trend of Tc migration reverses after 30 days suggesting that a fraction of the initially released ^{99}Tc is taken up in a later stage by the cement matrix. The likely cause is reduction of Tc(VII) to Tc(IV). The results of batch tests described above indicate that Tc(VII) is only weakly adsorbed onto any hydrated cement phase, including AFt. Therefore, the likely cause of Tc retardation is reduction of Tc(VII) to Tc(IV), and consequently, both the rate and extent of migration will depend upon the presence of reductants in the blend. Such behavior does not lend itself to a simple modelling description based on equilibrium partitioning of a tracer between solution and the solid phase.

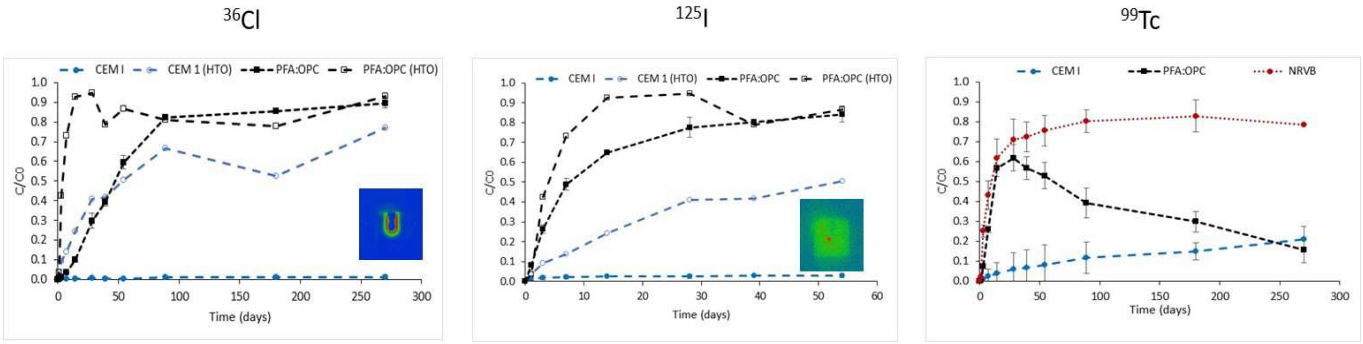

Figure 9: Break through curves of selected anionic species in HCP samples. Inserts are autoradiographic images for ^{36}Cl in CEMI and for ^{125}I in PFA HCP.

A set of diffusion experiments for ^{223}Ra and ^{85}Sr with a carrier (c_0 = 0.35 mmol·L^{-1}) was carried out for 3 weeks in Portlandite water or CPW through the CEM II/A-S 42.5 R layer (with a diffusion length of 0.5 cm) that was prepared unconventionally by pressing a crushed hydrated cement paste and saturated with the selected solution prior to the addition of the migrating element (Figure 10). The volume of the inlet and outlet reservoirs was 50 ml. The initial concentrations of both radionuclides were the same as for sorption experiments. The experimental time was limited because of the short half-life of the ^{223}Ra isotope. Consequently, the breakthrough of Ra did not occur.

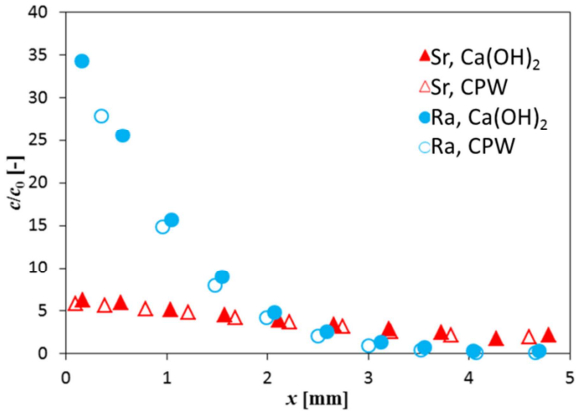

Figure 10: Concentration profiles (volumetric activity or concentration in both phases) of the sorbed elements in the CEM II/A-S 42.5 R HCP in contact with portlandite water (saturated $Ca(OH)_2$ solution) or synthetic cement water (CPW).

The determined R_d values, obtained by an original evaluation of through-diffusion experiments in the transient state were (Vopalka et al., 2019) around 9 $L \cdot kg^{-1}$ for Sr for both liquid phase used, 150 $L \cdot kg^{-1}$ for Ra in the portlandite water (slightly higher than in batch sorption studies, see table 2), and 100 L·kg for Ra in CPW. Based on the comparison of the dry sample weight with the sum of the weights of the cut slices generated at the end of the diffusion experiment it can be stated that $V \cdot m^{-1}$ phase ratio was equal to 0.3 $L \cdot kg^{-1}$. The results are in good agreement with the R_d values originating from sorption experiments.

Using tritiated water (HTO), diffusion properties for fully water-saturated CEM V samples were compared to those for unsaturated samples (Sw=0.85) and samples exposed to drying (55-80% RH) and rewetting cycles (for experimental conditions see supplementary material, 5). An effective diffusion coefficient D_e^{ref}(HTO) was obtained for a fully water saturated reference sample of CEM V of $3.94 \pm 0.4 \cdot 10^{-13}$ $m^2 \cdot s^{-1}$, in agreement with literature data (Savoye et al., 2018). For up to 70% RH, wet/drying cycles seems to have no influence on D_e(HTO), whereas for up to 55% RH, D_e(HTO) values increased slightly (D_e(HTO)=$5.1 \pm 0.5\ 10^{-13}$ $m^2 \cdot s^{-1}$). These data are interpreted as resulting from a mesoporosity which locally favours the transport of HTO in the pore network without modifying the total water accessible porosity. For unsaturated conditions (Sw=0.85), D_e(HTO)= $11 \pm 1 \cdot 10^{-13}$ $m^2 \cdot s^{-1}$, which is four times higher than the reference value (S_w=1), the opposite trend of what is expected. This may be explained by changes in HCP microstructure caused by osmosis; eg. microcracks forming due to locally heterogeneous desaturation but this has not yet been confirmed.

For carbonated HCP samples, the drying/rewetting cycle results in an increase of D_e(HTO) by a factor of three with respect to the reference sample. The result is consistent with the impact of carbonation on CEM V HCP as recently described by Auroy et al. (2015). Unlike Portland HCP, for which carbonation and precipitation of $CaCO_3$ leads to porosity clogging, for composite HCP, such as CEM V, the carbonation process induces the formation of microcracks (due to C-S-H decalcification, subsequent polymerization which generates shrinkage and eventually cracking). Globally, microcracks then act as a connected porosity network, accelerating HTO diffusion. Nevertheless, during through-diffusion experiments with fully saturated samples, conditions are favorable for a self-sealing process to occur in the microcrack network, thus reducing D_e(HTO) values.

The transport properties of $^{14}CO_3^{2-}$ in saturated and unsaturated carbonated CEM V samples was studied by digital autoradiography (Beaver system, AI4R, France) in order to estimate diffusion coefficients for ^{14}C. The experiments were run for approximatively 1 year. For the non-carbonated HCP sample, ^{14}C is located in a single zone at 200-300 µm depth below the surface (on the upstream side) giving an estimated diffusion depth for ^{14}C of 240 µm. For the carbonated HCP sample, ^{14}C penetrates more deeply into the sample; concentrated in a zone of 500 µm below the surface, again on the upstream side, followed by a more diffuse zone up to about 1.2 mm. The upper limit for a diffusion coefficient of ^{14}C is therefore,10^{-13} $m^2.s^{-1}$.

Conclusions

A large part of this work was focused on the role of AFm phases in anion retention. The thermodynamic properties of each of the pure AFm-Se and AFm-I phases were determined as well as AFm phases containing binary mixtures of Se and I with a common anions present in cement. Strong evidence was observed for the intercalation of sulfur, selenium and iodine anions in the AFm interlayers. Literature data from Ma et al. (2018) were confirmed showing that differences in basal spacing and crystal symmetry are due to the size and position of the interlayer anion as well as the hydration number of the anions.

Experimental data can sometimes be described in terms of both adsorption constant and by solid solution formation. The presence of Se in AFm systems leads in most cases to the formation of a new discrete Se-AFm phase. There could be miscibility gap between I-AFm and monocarbonate (AFm-CO_3). Limiting factors for solid solution formation are crystal symmetry, size of the interlayer anion and the hydration state of the phase. The uptake of iodate (IO_3) by AFt as well as by AFm-SO_4 led to iodate-substituted ettringite, formed either by anion exchange or phase transformation. New thermodynamic models have been derived, allowing a quantitative description of the sorption competition between the uptake of Se(VI), Se(IV) and I(-I) on AFm phases. The retention capacity for selenite and selenate is higher HCP based on CEM I than in the low–pH CEBAMA reference paste due to the higher proportion of aluminate phases in the former.

Exchange processes on AFm phases are fast; accurate rate laws have been determined which are readily implementable in reactive transport modelling. Diffusion experiments were performed with various anionic species ($^{36}Cl^-$, $^{99}TcO_4^-$, $^{125}I^-$, ^{14}C) or sorbing radionuclides (Ra, Sr) through saturated hardened cement pastes considering as well partially water saturated conditions.

The work has shown that the uptake of molybdenum by cements is not associated with ettringite, as often assumed. However, the data obtained and models derived still need to be tested with real concrete and integrated in reactive transport models.

The present work has provided a first set of sorption parameters for beryllium onto cementitious phases. In contrast to the traditional hypothesis of very weak Be sorption, assumed on the basis of the negative charge of the Be(II) species at high pH values, strong uptake has been confirmed for all systems investigated.

The results obtained provided an improved understanding of the behaviour of several safety relevant radionuclides within cementitious barriers in repository environment, thus decreasing uncertainties with respect to relevant radionuclide retention processes. The results can be used to substantiate and justify assumptions made with respect to radionuclide migration behavior in safety assessments.

Acknowledgement

SUBATECH acknowledges the strong help in experimental work by Katy Perrigaud et Niclolas Bessaguet.

Funding

The research leading to these results has received funding from the European Union's European Atomic Energy Community's (Euratom) Horizon 2020 Program (NFRP-2014/2015) under Grant Agreement, 662147 - Cebama".

References

Aimoz, L., Wieland, E., Taviot-Guého, C., Dähn, R., Vespa, M., Churakov, S.V., 2012. Structural insight into iodide uptake by AFm phases. Environ Sci Technol 46, 3874–3881. https://doi.org/10.1021/es204470e

Allen, P.G., Siemering, G.S., Shuh, D.K., Bucher, J.J., Edelstein, N.M., Langton, C.A., Clark, S., Reich, T., Denecke,

M., 1997. Technetium speciation in cement waste forms determined by X-ray absorption fine structure spectroscopy. Radiochim. Acta. 76, 77–86.
Allmann, R., 1977. Refinement of the hybrid layer structure [Ca2Al(OH)6]+·[1/2SO4·3H2O]-. Neues Jahrb. Mineral. Monatsh. 3, 136–144.
Atkins, M., Glasser, F.P., 1992. Application of portland cement-based materials to radioactive waste immobilization. Waste Management 12, 105–131. https://doi.org/10.1016/0956-053X(92)90044-J
Atkinson, A., Nickerson, A.K., 1984. The diffusion of ions through water-saturated cement. J Mater Sci 19, 3068–3078. https://doi.org/10.1007/BF01026986
Auroy, M., Poyet, S., Le Bescop, P., Torrenti, J.-M., Charpentier, T., Moskura, M., Bourbon, X., 2015. Impact of carbonation on unsaturated water transport properties of cement-based materials. Cement and Concrete Research 74, 44–58. https://doi.org/10.1016/j.cemconres.2015.04.002
Baur, I., Johnson, C.A., 2003. Sorption of Selenite and Selenate to Cement Minerals. Environ. Sci. Technol. 37, 3442–3447. https://doi.org/10.1021/es020148d
Berner, U., 2014. Solubility of Radionuclides in a Concrete Environment for Provisional Safety Analyses for SGT-E2 (No. 14– 07). NAGRA, CH-5430 Wettingen Switzerland.
Berner, U., 1999. Concentration Limits in the Cement Based Swiss Repository for Long-lived, Intermediate-level Radioactive Wastes (LMA) (PSI Bericht No. 99–10). Paul Scherrer Institut CH - 5232 Villigen PSI.
Bonhoure, I., Baur, I., Wieland, E., Johnson, C.A., Scheidegger, A.M., 2006. Uptake of Se(IV/VI) oxyanions by hardened cement paste and cement minerals: An X-ray absorption spectroscopy study. Cement and Concrete Research 36, 91–98.
Bonhoure, I., Scheidegger, A.M., Wieland, E., Dähn, R., 2002. Iodine species uptake by cement and CSH studied by I K-edge X-ray absorption spectroscopy. Radiochimica Acta 90. https://doi.org/10.1524/ract.2002.90.9-11_2002.647
Bradbury, M, Sarrot, F.A., 1995. Sorption Databases for the Cementitious Near-Field of a L/ILW Repository for Performance Assessment (PSI Bericht No. 95– 06). Paul Scherrer Institut.
Bruno, J., 1987. Beryllium(II) hydrolysis in 3.0 mol dm–3 perchlorate. J. Chem. Soc., Dalton Trans. 2431–2437. https://doi.org/10.1039/DT9870002431
Buttler, F.G., Dent Glasser, L.S., Taylor, H.F.W., 1959. Studies on 4CaOAl2.O3.13H2O and the Related Natural Mineral Hydrocalumite. J American Ceramic Society 42, 121–126. https://doi.org/10.1111/j.1151-2916.1959.tb14078.x
Cevirim-Papaioannou, N., Gaona, X., Altmaier, M., 2019. Thermodynamic description of Be(II) solubility and hydrolysis in acidic to hyperalkaline NaCl and KCl solutions,. Applied Geochemistry this issue.
Champenois, J.-B., Mesbah, A., Cau Dit Coumes, C., Renaudin, G., Leroux, F., Mercier, C., Revel, B., Damidot, D., 2012. Crystal structures of Boro-AFm and sBoro-AFt phases. Cement and Concrete Research 42, 1362–1370. https://doi.org/10.1016/j.cemconres.2012.06.003
Chinea, E., Dominguez, S., Mederos, A., Brito, F., Sanchez, A., Ienco, A., Vaca, A., 1997. Hydrolysis of beryllium(II) in DMSO:H2O. Main Group Metal Chemistry 20, 11–17.
Churakov, S.V., Labbez, C., Pegado, L., Sulpizi, M., 2014. Intrinsic Acidity of Surface Sites in Calcium Silicate Hydrates and Its Implication to Their Electrokinetic Properties. J. Phys. Chem. C 118, 11752–11762. https://doi.org/10.1021/jp502514a
Cornelis, G., Johnson, C.A., Gerven, T.V., Vandecasteele, C., 2008. Leaching mechanisms of oxyanionic metalloid and metal species in alkaline solid wastes: A review. Applied Geochemistry 23, 955–976. https://doi.org/10.1016/j.apgeochem.2008.02.001
Es, E. van, Hinchliff, J., Felipe-Sotelo, M., Milodowski, A.E., Field, L.P., Evans, N.D.M., Read, D., 2015. Retention of chlorine-36 by a cementitious backfill. Mineralogical Magazine 79, 1297–1305. https://doi.org/10.1180/minmag.2015.079.6.05
Evans, N.D.M., 2008. Binding mechanisms of radionuclides to cement. Cement and Concrete Research, 38, 543–553.
Favre-Nicolin, V., Černý, R., 2002. FOX, `free objects for crystallography': a modular approach to ab initio structure determination from powder diffraction. J Appl Cryst 35, 734–743. https://doi.org/10.1107/S0021889802015236
Felipe-Sotelo, M., Hinchliff, J., Drury, D., Evans, N.D.M., Williams, S., Read, D., 2014. Radial diffusion of radiocaesium and radioiodide through cementitious backfill. Physics and Chemistry of the Earth Complete, 60–70. https://doi.org/10.1016/j.pce.2014.04.001
Felipe-Sotelo, M., Hinchliff, J., Evans, N.D.M., Read, D., 2016. Solubility constraints affecting the migration of selenium through the cementitious backfill of a geological disposal facility. Journal of Hazardous Materials 305, 21–29. https://doi.org/10.1016/j.jhazmat.2015.11.024

Felipe-Sotelo, M., Hinchliff, J., Field, L.P., Milodowski, A.E., Preedy, O., Read, D., 2017. Retardation of uranium and thorium by a cementitious backfill developed for radioactive waste disposal. Chemosphere 179, 127–138. https://doi.org/10.1016/j.chemosphere.2017.03.109

Giffaut, E., Grivé, M., Blanc, P., Vieillard, P., Colàs, E., Gailhanou, H., Gaboreau, S., Marty, N., Madé, B., Duro, L., 2014. Andra thermodynamic database for performance assessment: ThermoChimie. Applied Geochemistry, Geochemistry for Risk Assessment: Hazardous waste in the Geosphere 49, 225–236. https://doi.org/10.1016/j.apgeochem.2014.05.007

Glasser, F.P., Macphee, D., Atkins, M., Pointer, C., Cowie, J., Wilding, C.R., Mattingley, N.J., Evans, P.A., 1989. Immobilisation of radwaste in cement based matrices (No. DOE-RW--89.058). Department of the Environment.

Goetz-Neunhoeffer, F., Neubauer, J., 2006. Refined ettringite ($Ca_6Al_2(SO_4)_3(OH)_{12}\cdot 26H_2O$) structure for quantitative X-ray diffraction analysis. Powder Diffr. 21, 4–11. https://doi.org/10.1154/1.2146207

Grangeon, S., Marty, N., 2019. in press.

Grive, M., Olmeda, J., 2016. Molybdenum behaviour in cementitious materials. CEBAMA state of the art report.

Henocq, P., Robinet, J.C., Perraud, D., Munier, I., et al., 2018. CArbon-14 Source Term CAST, – Integration of CAST results to safety assessment (Deliverable of EU project CAST No. D 6.3).

Hillier, S., Lumsdon, D.G., Brydson, R., Paterson, E., 2007. Hydrogarnet: A Host Phase for Cr(VI) in Chromite Ore Processing Residue (COPR) and Other High pH Wastes. Environ. Sci. Technol. 41, 1921–1927. https://doi.org/10.1021/es0621997

Hummel, W., Berner, U., Curti, E., Pearson, F.J., Thoenen, T., 2002a. Nagra/PSI Chemical Thermodynamic Data Base 01/01. Radiochimica Acta 90. https://doi.org/10.1524/ract.2002.90.9-11_2002.805

Hummel, W., Berner, U., Curti, E., Pearson, F.J., Thoenen, T., 2002b. Nagra/PSI Chemical Thermodynamic Data Base 01/01. Universal Publisher/uPublish.com, Parkland, Florida.

Jenkins, Thakur, 1979. Reappraisal of thermochemical radii for complex ions. J. Chem. Educ. 56, 576.

Johnson, E.A., Rudin, M.J., Steinberg, S.M., Johnson, W.H., 2000. The sorption of selenite on various cement formulations. Waste Management 20, 509–516. https://doi.org/10.1016/S0956-053X(00)00024-6

Kakihana, H., Sillen, G., 1956. Studies on the Hydrolysis of Metal Ions. XVI. The Hydrolysis of the Beryllium Ion, Be2+. Acta Chemica Scandinavica 10, 985–1005.

Kindness, A., Lachowski, E.E., Minocha, A.K., Glasser, F.P., 1994. Immobilisation and fixation of molybdenum (VI) by Portland cement. Waste Management 14, 97–102. https://doi.org/10.1016/0956-053X(94)90002-7

Kulik, D.A., Wagner, T., Dmytrieva, S.V., Kosakowski, G., Hingerl, F.F., Chudnenko, K.V., Berner, U., 2013. GEM-Selektor geochemical modeling package: Revised algorithm and GEMS3K numerical kernel for coupled simulation codes. Computational Geosciences 17, 1–24. https://doi.org/10.1007/s10596-012-9310-6

Lange, S., Kowalski, P.M., Pšenička, M., Klinkenberg, M., Rohmen, S., Bosbach, D., Deissmann, G., 2018. Uptake of 226Ra in cementitious systems: A complementary solution chemistry and atomistic simulation study. Applied Geochemistry 96, 204–216. https://doi.org/10.1016/j.apgeochem.2018.06.015

Luksic, S.A., Riley, B.J., Schweiger, M., Hrma, P., 2015. Incorporating technetium in minerals and other solids: A review. Journal of Nuclear Materials 466, 526–538. https://doi.org/10.1016/j.jnucmat.2015.08.052

Ma, B., Charlet, L., Fernandez-Martinez, A., Kang, M., Madé, B., 2019. A review of the retention mechanisms of redox-sensitive radionuclides in multi-barrier systems. Applied Geochemistry 100, 414–431. https://doi.org/10.1016/j.apgeochem.2018.12.001

Ma, B., Fernandez-Martinez, A., Grangeon, S., Tournassat, C., Findling, N., Carrero, S., Tisserand, D., Bureau, S., Elkaïm, E., Marini, C., Aquilanti, G., Koishi, A., Marty, N.C.M., Charlet, L., 2018. Selenite Uptake by Ca–Al LDH: A Description of Intercalated Anion Coordination Geometries. Environ. Sci. Technol. 52, 1624–1632. https://doi.org/10.1021/acs.est.7b04644

Ma, B., Fernandez-Martinez, A., Grangeon, S., Tournassat, C., Findling, N., Claret, F., Koishi, A., Marty, N.C.M., Tisserand, D., Bureau, S., Salas-Colera, E., Elkaïm, E., Marini, C., Charlet, L., 2017. Evidence of Multiple Sorption Modes in Layered Double Hydroxides Using Mo As Structural Probe. Environ. Sci. Technol. 51, 5531–5540. https://doi.org/10.1021/acs.est.7b00946

Mace, N., Landesman, C., Pointeau, I., Grambow, B., Giffaut, E., 2007. Characterisation of thermally altered cement pastes. Influence on selenite sorption. Advances in Cement Research. https://doi.org/10.1680/adcr.2007.19.4.157

Marty, N.C.M., Grangeon, S., Elkaïm, E., Tournassat, C., Fauchet, C., Claret, F., 2018. Thermodynamic and crystallographic model for anion uptake by hydrated calcium aluminate (AFm): an example of molybdenum. Scientific Reports 8, 7943. https://doi.org/10.1038/s41598-018-26211-z

Marty, N.C.M., Grangeon, S., Lerouge, C., Warmont, F., Rozenbaum, O., Conte, T., Claret, F., 2017. Dissolution kinetics of hydrated calcium aluminates (AFm-Cl) as a function of pH and at room temperature. Mineral.

mag. 81, 1245–1259. https://doi.org/10.1180/minmag.2016.080.161
Mattigod, S.V., Whyatt, G.A., Serne, R.J., Martin, P.F., Schwab, K.E., Wood, M.I., 2001. Diffusion and Leaching of Selected Radionuclides (Iodine-129, Technetium-99, and Uranium) Through Category 3 Waste Encasement Concrete and Soil Fill Material (No. PNNL-13639). Pacific Northwest National Laboratory, Richland, Wa 99352, USA.
Mesbah, A., Cau-dit-Coumes, C., Frizon, F., Leroux, F., Ravaux, J., Renaudin, G., 2011. A New Investigation of the Cl−−CO32− Substitution in AFm Phases. Journal of the American Ceramic Society 94, 1901–1910. https://doi.org/10.1111/j.1551-2916.2010.04305.x
Missana, T., García-Gutiérrez, M., Mingarro, M., Alonso, U., 2017. Analysis of barium retention mechanisms on calcium silicate hydrate phases. Cement and Concrete Research 93, 8–16. https://doi.org/10.1016/j.cemconres.2016.12.004
Nedyalkova, L., Lothebach, B., Geng, G., Mäder, U., Tits, J., 2019. Uptake of iodide by carbonate-bearing calcium aluminate phases (AFm phases). Applied Geochemistry submitted.
Nedyalkova, Latina, Lothenbach, B., Renaudin, G., Mäder, U., Tits, J., 2019. Effect of redox conditions on the structure and solubility of sulfur- and selenium-AFm phases. Cement and Concrete Research 123, 105803. https://doi.org/10.1016/j.cemconres.2019.105803
Noshita, K., Nishi, T., Matsuda, M., Izumida, T., 1995. Sorption Mechanism of Carbon-14 by Hardened Cement Paste. MRS Online Proceedings Library Archive 412. https://doi.org/10.1557/PROC-412-435
Ochs, M., Mailants, D., Wang,L., 2016. Radionuclide and Metal Sorption on Cement and Concrete. Springer, Cham.
Olmeda, J., Missana, T., Grandia, F., Grivé, M., García-Gutiérrez, M., Mingarro, M., Alonso, U., Colàs, E., Henocq, P., Munier, I., Robinet, J.C., 2019. Radium retention by blended cement pastes and pure phases (C-S-H and C-A-S-H gels): Experimental assessment and modelling exercises. Applied Geochemistry 105, 45–54. https://doi.org/10.1016/j.apgeochem.2019.04.004
Pointeau, I., Coreau, N., Reiller, P.E., 2008. Uptake of anionic radionuclides onto degraded cement pastes and competing effect of organic ligands. Radiochimica Acta 96, 367–374.
Pointeau, I., Reiller, P., Macé, N., Landesman, C., Coreau, N., 2006. Measurement and modeling of the surface potential evolution of hydrated cement pastes as a function of degradation. Journal of Colloid and Interface Science 300, 33–44. https://doi.org/10.1016/j.jcis.2006.03.018
Rojo, H., Scheinost, A.C., Lothenbach, B., Laube, A., Wieland, E., Tits, J., 2018. Retention of selenium by calcium aluminate hydrate (AFm) phases under strongly-reducing radioactive waste repository conditions. Dalton Trans. 47, 4209–4218. https://doi.org/10.1039/C7DT04824F
Sarott, F.-A., Bradbury, M.H., Pandolfo, P., Spieler, P., 1992. Diffusion and adsorption studies on hardened cement paste and the effect of carbonation on diffusion rates. Cement and Concrete Research, Special Double Issue Proceedings of Symposium D of the E-MRS Fall Meeting 1991 22, 439–444. https://doi.org/10.1016/0008-8846(92)90086-B
Savoye, S., Rajyaguru, A., Macé, N., Lefèvre, S., Spir, G., Robinet, J.C., 2018. How mobile is tritiated water through unsaturated cement-based materials? New insights from two complementary approaches. Appl Radiat Isot 139, 98–106. https://doi.org/10.1016/j.apradiso.2018.04.019
Solem-Tishmack, J.K., McCarthy, G.J., Docktor, B., Eylands, K.E., Thompson, J.S., Hassett, D.J., 1995. High-calcium coal combustion by-products: Engineering properties, ettringite formation, and potential application in solidification and stabilization of selenium and boron. Cement and Concrete Research 25, 658–670. https://doi.org/10.1016/0008-8846(95)00054-G
Taylor, T., 1997. Cement-Chemistry - 2nd Edition.
Tits, J., Iijima, K., Kamei, G., Wieland, E., 2006a. The uptake of radium by calcium silicate hydrates and hardened cement paste. Radiochimica Acta 94, 637–643.
Tits, J., Wieland, E., Müller, C.J., Landesman, C., Bradbury, M.H., 2006b. Strontium binding by calcium silicate hydrates. Journal of Colloid and Interface Science 300, 78–87. https://doi.org/10.1016/j.jcis.2006.03.043
Vopalka, D., Rosendorf, T., Barborova, L., Kitternova, J., 2019. Modelling and interpretation of diffusion experiments of selected radionuclides through cementitious samples. Final results and interpretation of the modelling of experiments within CEBAMA (No. (https://www.cebama.eu/Content/PublicArea/WP3/D3.06.pdf)).
Walker, C., 2010. C-S-H gel models (in PHREEQC), 3rd GEMS workshop, Thermodynamic modeling in cementitious systems, Dubendorf, Switzerland.
Wieland, E., 2014. Sorption Data Base for the Cementitious Near Field of L/ILW and ILW Repositories for Provisional Safety Analyses for SGT-E2 (No. 14– 08), Nagra Technical Report. CH-5430 Wettingen Switzerland.

Wieland, E., Van Loon, L., 2003. Cementitious Near-Field Sorption Data Base for Performance Assessment of an ILW Repository in Opalinus Clay (No. PSI Bericht Nr . 03-06). Paul Scherrer Institut, CH-5232 Villigen PSI.

Zhang, M., Reardon, E.J., 2003. Removal of B, Cr, Mo, and Se from wastewater by incorporation into hydrocalumite and ettringite. Environ. Sci. Technol. 37, 2947–2952.

Zingg, A., Winnefeld, F., Holzer, L., Pakusch, J., Becker, S., Gauckler, L., 2008. Adsorption of polyelectrolytes and its influence on the rheology, zeta potential, and microstructure of various cement and hydrate phases. Journal of Colloid and Interface Science 323, 301–312. https://doi.org/10.1016/j.jcis.2008.04.052

Highlights

- understanding of retention processes of anions on cementitious materials
- decreasing uncertainties with respect to radionuclide on cementitious materials
- justifying assumptions for radionuclide migration in safety assessments
- improving sorption databases for fresh and degraded cement systems

Declaration of interests

☒ The authors declare that they have no known competing financial interests or personal relationships that could have appeared to influence the work reported in this paper.

☐The authors declare the following financial interests/personal relationships which may be considered as potential competing interests: